An AzTEC 1.1-mm Survey for ULIRGs in the field of the Galaxy Cluster MS 0451.6−0305

J. L. Wardlow[1]⋆, Ian Smail[2], G. W. Wilson[3], M. S. Yun[3], K. E. K. Coppin[2], R. Cybulski[3], J. E. Geach[1], R. J. Ivison[4,5], I. Aretxaga[6], J. E. Austermann[7], A. C. Edge[2], G. G. Fazio[8], J. Huang[8], D. H. Hughes[6], T. Kodama[9], Y. Kang[10], S. Kim[10], P. D. Mauskopf[11], T. A. Perera[12], K. S. Scott[3,13]

[1]*Department of Physics, Durham University, South Road, Durham, DH1 3LE, UK*
[2]*Institute for Computational Cosmology, Durham University, South Road, Durham, DH1 3LE, UK*
[3]*Department of Astronomy, University of Massachusetts, Amherst, MA 01003, USA*
[4]*Scottish Universities Physics Alliance, Institute for Astronomy, University of Edinburgh, Blackford Hill, Edinburgh, EH9 3HJ, UK*
[5]*UK Astronomy Technology Centre, Royal Observatory, Blackford Hill, Edinburgh EH9 3HJ, UK*
[6]*Instituto Nacional de Astrofísica, Óptica y Electrónica, Tonantzintla, Puebla, México*
[7]*Center for Astrophysics and Space Astronomy, University of Colorado, Boulder, CO 80309, USA*
[8]*Harvard-Smithsonian Center for Astrophysics, 60 Garden St. MS-65, Cambridge, MA 02138-1516, USA*
[9]*National Astronomical Observatory of Japan, Mitaka, Tokyo 181-8588, Japan*
[10]*Astronomy & Space Science Department, Sejong University, Seoul, South Korea*
[11]*School of Physics & Astronomy, Cardiff University, Queens Buildings, The Parade, Cardiff, CF24 3AA, UK*
[12] *Illinois Wesleyan University, P.O. Box 2900, Bloomington, IL 61702-2900, USA*
[13] *Department of Physics and Astronomy, University of Pennsylvania, Philadelphia, PA 19104, USA*

ABSTRACT

We have undertaken a deep ($\sigma \sim 1.1$ mJy) 1.1-mm survey of the $z = 0.54$ cluster MS 0451.6−0305 using the AzTEC camera on the James Clerk Maxwell Telescope. We detect 36 sources with S/N $\geqslant 3.5$ in the central 0.10 deg^2 and present the AzTEC map, catalogue and number counts. We identify counterparts to 18 sources (50%) using radio, mid-infrared, *Spitzer* IRAC and Submillimeter Array data. Optical, near- and mid-infrared spectral energy distributions are compiled for the 14 of these galaxies with detectable counterparts, which are expected to contain all likely cluster members. We then use photometric redshifts and colour selection to separate background galaxies from potential cluster members and test the reliability of this technique using archival observations of submillimetre galaxies. We find two potential MS 0451−03 members, which, if they are both cluster galaxies have a total star-formation rate (SFR) of ~ 100 M$_\odot$yr^{-1} – a significant fraction of the combined SFR of all the other galaxies in MS 0451−03. We also examine the stacked rest-frame mid-infrared, millimetre and radio emission of cluster members below our AzTEC detection limit and find that the SFRs of mid-IR selected galaxies in the cluster and redshift-matched field populations are comparable. In contrast, the average SFR of the morphologically classified late-type cluster population is ~ 3 times less than the corresponding redshift-matched field galaxies. This suggests that these galaxies may be in the process of being transformed on the red-sequence by the cluster environment. Our survey demonstrates that although the environment of MS 0451−03 appears to suppress star-formation in late-type galaxies, it can support active, dust-obscured mid-IR galaxies and potentially millimetre-detected LIRGs.

Key words: submillimetre – galaxies: clusters: individual (MS 0451−03).

1 INTRODUCTION

Galaxy clusters are highly biased environments in which galaxies potentially evolve more rapidly than in the field. The galaxy populations of local massive clusters contain mainly early-

⋆ E-mail: j.l.wardlow@durham.ac.uk

type galaxies which define a colour-magnitude relation (CMR) (Visvanathan & Sandage 1977; Bower et al. 1992). However, studies of clusters out to $z \sim 1$ suggest that they contain increasing activity at higher redshifts due to a growing fraction of blue, star-forming galaxies (Butcher & Oemler 1984). Over the same redshift range there appears to be a growing deficit in the CMR population at faint magnitudes, as well as a claimed increasing decline in the numbers of S0 galaxies, suggesting that the blue, star-forming galaxies may be transforming into these passive populations with time (Dressler et al. 1997; Smail et al. 1998; De Lucia et al. 2007; Stott et al. 2007; Holden et al. 2009).

The blue, star-forming populations within the clusters are accreted from the surrounding field as the clusters grow via gravitational collapse. The evolution in the star-forming fraction in the clusters may thus simply track the increasing activity in the field population at higher redshifts. The increasing activity in the field is also reflected in an increasing number of the most luminous (and dusty) star-burst galaxies with redshift (e.g. Le Floc'h et al. 2005): the Luminous Infrared Galaxies (with $L_{FIR} \geqslant 10^{11} \, L_{\odot}$) and their Ultraluminous cousins (ULIRGs, $L_{FIR} \geqslant 10^{12} \, L_{\odot}$). These systems will also be accreted into the cluster environment along with their less-obscured and less-active population as the clusters grow. Indeed, mid-infrared (mid-IR) surveys of clusters have identified a population of dusty star-bursts whose activity increases with redshift (e.g. Geach et al. 2006, 2008). However, these mid-IR surveys can miss the most obscured (and potentially most active) galaxies which are optically thick in the rest-frame mid-IR. If they are present in clusters – even in relatively low numbers – such active galaxies will contribute significantly to the star formation rate (SFR) in these environments and the metal enrichment of the intracluster medium. Hence to obtain a complete census of the star formation within clusters we need to survey these systems at even longer wavelengths, in the rest-frame far-infrared (far-IR), corresponding to the observed sub-millimetre and millimetre waveband.

Over the past decade or more there have been a number of studies of rich clusters of galaxies in the sub-millimetre and millimetre wavebands (e.g. Smail et al. 1997; Zemcov et al. 2007; Knudsen et al. 2008). Many of these studies were seeking to exploit the clusters as gravitational telescopes to aid in the study of the distant sub-millimetre galaxy (SMG) population behind the clusters, while others focused on the detection of the Sunyaev-Zel'dovich (SZ) emission. Due to the limitations of current technologies direct detection of millimetre sources is restricted to those with fluxes $S_{1100\mu m} \gtrsim 1$ mJy, or equivalently galaxies with SFRs $\gtrsim 300 \, M_{\odot} \, yr^{-1}$ – much higher than expected for the general cluster populations based on optical surveys. Nevertheless these studies have serendipitously detected a number of cluster galaxies, although these are either atypical (e.g. central cluster galaxies, Edge et al. (1999)) or are not confirmed members (e.g. Best 2002; Webb et al. 2005). More critically, with few exceptions these studies have all focused on the central 2–3 arcmin of the clusters, where the SZ emission and lensing amplification both peak, and have not surveyed the wider environment of the cluster outskirts where much of the obscured star formation is likely to be occurring (e.g. Geach et al. 2006). The two exceptions are the wide-field survey of the $z \sim 0.25$ cluster A 2125 by Wagg et al. (2009) and the survey of an overdense region of the COSMOS field by Scott et al. (2008) and Austermann et al. (2009a). Wagg et al. (2009) detected 29 millimetre galaxies across a ~ 25-arcmin diameter region centered on A 2125 of which none are claimed to be members. However, the only redshift estimates available are based on crude radio-to-millimetre spectral indices, which are sensitive to both dust tem-

perature and redshift (Blain et al. 2003). The AzTEC/COSMOS survey (Scott et al. 2008; Austermann et al. 2009a) covered a number of structures, including an X-ray detected $z = 0.73$ cluster and concluded that the statistical overdensity of sources was most likely due to the gravitational lensing of background SMGs by these foreground structures.

To help to conclusively answer the issue of the obscured star-forming populations in distant clusters we have therefore undertaken a wide-field 1.1-mm survey of the $z = 0.54$ rich cluster MS 0451.6−0305 (hereafter MS 0451−03) with the AzTEC camera (Wilson et al. 2008) on the James Clerk Maxwell Telescope (JCMT). This panoramic millimetre survey can also take advantage of the significant archival data available for this well-studied region. In particular the panoramic imaging of MS 0451−03 from *Spitzer* and uniquely, the *Hubble Space Telescope* (*HST*), as well as extensive archival multiwavelength imaging and spectroscopy, which we employ for determining cluster membership of AzTEC-detected galaxies. Our survey probes the rest-frame 700 μm emission of cluster galaxies – in search of examples of strongly star-forming but obscured galaxies – as well as identifying more luminous and more distant examples of the SMG population. We can compare our millimetre search for cluster members to the previous mid-IR survey of this cluster by Geach et al. (2006) who uncovered a population of dusty star-forming galaxies which dominate the integrated SFR of the cluster of $200 \pm 100 \, M_{\odot} \, yr^{-1}$. Our AzTEC map covers ~ 60 times the area of the 850 μm SCUBA observations of the central region of MS 0451−03 (Borys et al. 2004b), while the depth of $\sigma \sim 1.1$ mJy is sufficient to identify ULIRGs individually and obtain stacked constraints on far-IR fainter cluster members.

We describe our observations and the data reduction in §2; present 1.1-mm number counts, identify counterparts to the AzTEC galaxies, and use photometric techniques to determine cluster membership in §3. §4 contains our conclusions; individual AzTEC galaxies are presented in Appendix A. Throughout this paper we use J2000 coordinates and ΛCDM cosmology with $\Omega_M = 0.3$, $\Omega_{\Lambda} = 0.7$ and $H_0 = 70$ kms^{-1}Mpc^{-1} and all photometry is on the AB system unless otherwise stated.

2 OBSERVATIONS AND DATA REDUCTION

2.1 AzTEC Observations

The AzTEC millimetre camera (Wilson et al. 2008) was installed on the JCMT during November 2005 and operated nearly continuously until February 2006. On the JCMT AzTEC has a field-of-view of ~ 18-arcmin^2 and a beam of 18-arcsec FWHM. For this project we observed a 0.23-deg^2 region centred on MS 0451−03 at $04^h 54^m 10\overset{s}{.}1$, $03°01'07\overset{''}{.}6$, over a total of 24.5 hours between 2005 December 14 and 2006 January 6. Observations were carried out in raster-scan mode with $1200''$ long scans in elevation separated by $9''$ steps in azimuth (see Wilson et al. (2008) for details of our standard raster scan strategy). Scans were made at a fixed speed of $120'' s^{-1}$. Data from the turnarounds were excised for this analysis. Each observation took 35 minutes to complete and a total of 42 observations were made of the field. Over the set of observations the zenith opacity at 225 GHz, τ_{225}, was monitored with the Caltech Submillimeter Observatory's opacity meter and ranged from 0.03 to 0.17. The average opacity for the set of observations was 0.09, equivalent to an atmospheric column of precipitable water vapour of ~ 2 mm.
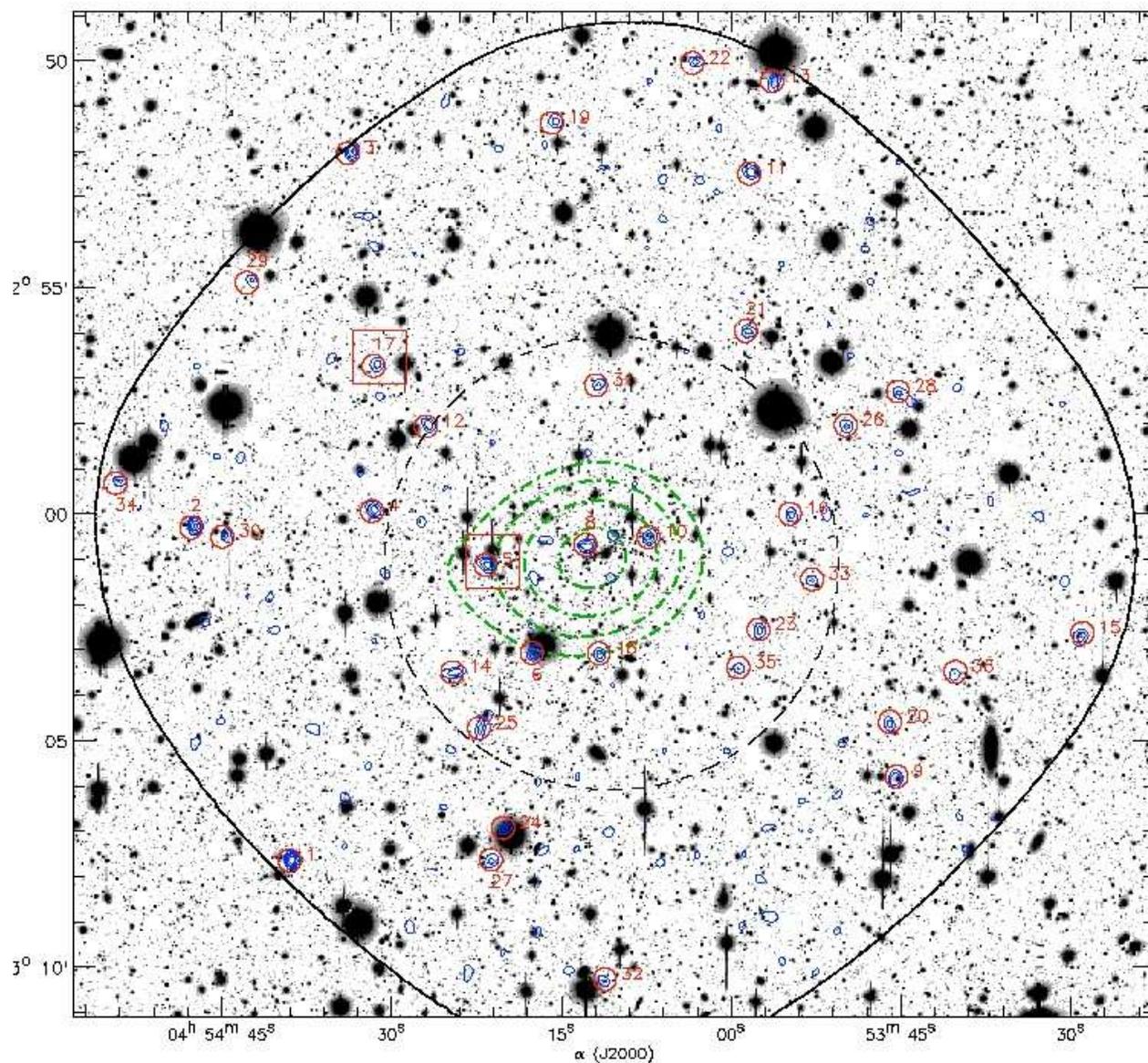
Figure 1. AzTEC S/N contours for the MS 0451−03 field shown over the corresponding Subaru *R*-band image; smoothed (dot-dashed) X-ray contours highlight the cluster centre. We also plot a 5-arcmin radius circle (dashed) illustrating the sub-region analysed in §3.1. The solid black line encircles the region with exposure coverage $\geqslant 50\%$ of the maximum value, where sources are extracted. In this region AzTEC contours shown are at 1σ intervals, starting at 2.5σ. 15 arcsec radius circles mark the 1.1-mm source detections labelled in order of decreasing S/N (Table 2) and squares highlight sources which are potential cluster members (§3.3.3). MMJ 045413.35 is not shown because it lies outside of the area covered by the Subaru image. The 1.1-mm sources appear evenly distributed, with no obvious overdensity towards the cluster centre.

The 42 individual AzTEC observations were reduced and combined using the publicly available AzTEC Data Reduction Pipeline V1.0 – a set of IDL code that is optimised for detecting point sources in blank-field AzTEC surveys. This is the same pipeline that has been used in previous blank-field AzTEC/JCMT analyses including Scott et al. (2008), Perera et al. (2008) and Austermann et al. (2009b).

Since the reduction of these observations follows the same

procedure and uses the same code as previous AzTEC studies, we refer the reader to Scott et al. (2008) for a thorough review of the reduction steps. Here we focus on the particulars of this field and the measured characteristics of the MS 0451−03 map.

Since we are interested in counterparts to our detected SMGs it is critical that we understand the pointing accuracy of the maps. In the reduction pipeline, fine corrections to the JCMT's pointing model are applied to each observation based on reg-

ular observations of a nearby QSO ($\alpha = 04^{\mathrm{h}}23^{\mathrm{m}}15\overset{\mathrm{s}}{.}8, \delta = -01°20'33\overset{''}{.}1$) in the same manner as described in Scott et al. (2008) and Wilson et al. (2008). The residual astrometric error for the field is measured by stacking the AzTEC map at the positions of radio sources in the field (see §2.2) and fitting for the centroid of the resulting image. The stacked radio sources are detected at $\sim 6\sigma$ and demonstrate an overall systematic astrometric shift in the AzTEC map of $\Delta\alpha = -3.0'' \pm 0.9'', \Delta\delta = 1.2'' \pm 1.5''$ with respect to the radio reference frame. This correction is negligible in Dec, but the significant RA offset is applied to the AzTEC data prior to further analysis and source extraction.

The AzTEC data are flux calibrated as described in Wilson et al. (2008) from nightly observations of Uranus over the JCMT run. The final calibration accuracy is $\sim 10\%$.

The primary products which come out of the AzTEC pipeline are a map representing the average filtered point source response, a map of the of the weight of each pixel in the sky flux map (representing the uncertainty in flux of each pixel), and a map of the signal to noise estimate in each pixel. All maps are made on the same $3'' \times 3''$ grid and all maps have been Wiener filtered to optimize sensitivity to point sources. The central ~ 0.10 deg^2 of the AzTEC map is relatively uniform, with all pixels having $\geqslant 50\%$ of the peak weight. Sources are extracted in the central region of the maps (§3.1) where the rms noise is ~ 1.1 mJy. Contours of 'signal-to-noise' (S/N), overlaid on the Subaru R-band image of the field are shown in Fig. 1.

2.2   Multi-wavelength data

Significant multiwavelength archival data exist for the MS 0451−03 field, which are summarised in Table 1 and described below.

2.2.1   Spitzer MIPS imaging

Geach et al. (2006) obtained *Spitzer* MIPS 24μm observations of a 0.23-deg^2 area of MS 0451−03, excluding the central 25-arcmin^2. The full details of the reduction and source extraction process are described in Geach et al. (2006). The central region of the cluster was part of Guaranteed Time Observations (*Spitzer* program 83) so these data were obtained from the archive and incorporated into the mosaic. The 5-σ catalogue detection limit corresponds to 200 μJy.

2.2.2   Radio Imaging

Archival observations of the MS 0451−03 field at 1.4 GHz were obtained using the National Radio Astronomy Observatory's (NRAO[1]) Very Large Array (VLA), combining 9 hours of data obtained in 2002 June in the VLA's BnA configuration with 16 hours of A-configuration data taken in 2006 February (Project IDs AN109 and AB1199, respectively). The nearby calibrator, 0503+020, was used to track amplitude and phase, with absolute flux and bandpass calibration set via 0137+331. The now-standard 1.4-GHz wide-field imaging approach was adopted (Owen et al. 2005; Biggs & Ivison 2006), using spectral-line mode '4' to acquire data with an integration time of 3 s (10 s in BnA) and using the IMAGR task in the Astronomical Image Processing System (AIPS) to map out the primary beam using a mosaic of 37 images, with 17

---

[1] NRAO is operated by Associated Universities Inc., under a cooperative agreement with the National Science Foundation.

more distant radio sources covered by additional facets. Several iterations of self-calibration and imaging resulted in a noise level of 11 μJy beam^{-1}, with a $2.3'' \times 1.8''$ synthesised beam at a position angle 0.0°.

Sources and corresponding fluxes are obtained from SEXTRACTOR (Bertin & Arnouts 1996), using the S/N map for detection and the flux map as the analysis image; sources are extracted where a minimum of 10 contiguous pixels (each is 0.16 arcsec^2) have S/N$\geqslant$ 2. The resulting catalogue has a 3-σ flux limit of 51 μJy and is corrected for bandwidth smearing. We verify the statistical properties of our catalogue by comparing source counts with Biggs & Ivison (2006). Notably, the source density is not significantly enhanced towards the cluster centre, allowing us to use the counts across the whole field in our statistical calculation of AzTEC counterparts (§3.2.2).

2.2.3   Optical and near-infrared imaging

Observations of MS 0451−03 in the *U*-band were taken with the MegaPrime camera on the Canada France Hawaii Telescope (CFHT) and reach a 3-σ detection limit of 25.1 mag in a 0.25-deg^2 field. Standard reduction techniques were employed, customised for MegaPrime data (C.-J. Ma & H. Ebeling, private communication), details of which can be found in Donovan (2007).

In addition we observed a 0.08-deg^2 area centered on the cluster core on 2007 October 09 through the z' filter with the Prime Focus Imaging Platform mounted on the 4.2-m William Herschel Telescope (WHT). A total integration time of one hour was obtained and reduced using standard techniques and calibrated using a Sloan Digital Sky Survey standard field, yielding a 3-σ limiting magnitude of 24.2 mag.

Finally, the *BVRI* imaging employed here comes from the PISCES survey (Panoramic Imaging and Spectroscopy of Cluster Evolution with Subaru; Kodama et al. 2005). Detection limits are listed in Table 1. In addition *K*-band imaging to a 3-σ depth of 20.1 mag over 0.12-deg^2 centred on MS 0451−03 was obtained from the Wide-Field Infrared Camera (WIRC; Wilson et al. 2003) on the Palomar Hale telescope. Standard reduction methods were employed and are detailed in G. Smith et al. (in prep.). These data were used in the previous analyses of Geach et al. (2006) and Moran et al. (2007a,b).

2.2.4   Spitzer IRAC imaging

The *Spitzer* InfraRed Array Camera (IRAC; Fazio et al. 2004) observations of the $20' \times 20'$ field centered on the MS0451 field were obtained as a part of the Cycle 5 General Observer (program 50610, PI: M. Yun) on 2009 March 18. Each tile was observed for a total of 1500 seconds in each of the four IRAC bands (3.6, 4.5, 5.8, and 8.0 μm) in full array mode with a 15 position dither pattern with 100 second exposures at each position. The new data are combined with the archival IRAC data (program 83) to produce the final mosaic images using CLUSTER GRINDER (Gutermuth et al. 2009), which is an IDL software package that utilizes standard Basic Calibrated Data (BCD) products from the Spitzer Science Centre's standard data pipeline. The angular resolution of the final mosaic ranges between 2.0 to 2.5 arcsec depending on the observing band; the limiting depths are given in Table 1.

Table 1. Summary of the observations

Filter	Instrument	Detection Limit [a]	Reference
U	CFHT – MegaPrime	25.1 mag	Donovan (2007)
B	Subaru – Suprime-Cam	26.6 mag	Kodama et al. (2005)
V	Subaru – Suprime-Cam	25.8 mag	Kodama et al. (2005)
R	Subaru – Suprime-Cam	25.1 mag	Kodama et al. (2005)
I	Subaru – Suprime-Cam	24.2 mag	Kodama et al. (2005)
z'	WHT – PFIP	24.2 mag	This work
K	Palomar Hale – WIRC	20.1 mag	G. Smith et al., in prep.
3.6 μm	*Spitzer* – IRAC	23.0 mag	This work
4.5 μm	*Spitzer* – IRAC	23.2 mag	This work
5.8 μm	*Spitzer* – IRAC	21.4 mag	This work
8.0 μm	*Spitzer* – IRAC	22.1 mag	This work
24 μm	*Spitzer* – MIPS	120 μJy	Geach et al. (2006)
1.1 mm	JCMT – AzTEC	3.6 mJy	This work
1.4 GHz	VLA	51 μJy	This work

[a] 1.1 mm is the 3.5σ minimum catalogue limit in the roughly constant noise region of the map; in the other bands we quote 3σ limits.

2.2.5 Cataloguing

To estimate redshifts photometrically we require that the photometry in all filters samples the same emission from the source so an accurate spectral energy distribution (SED) can be built. To meet this requirement we degrade all the optical images to match the worst seeing – the (*V*-band) in which the FWHM is 1.54 arcsec. Each seeing convolved image is astrometrically matched to the USNO catalogue with a set of unsaturated and unblended stars spread across the frames. We use SEXTRACTOR (Bertin & Arnouts 1996) on the *R*-band image to detect objects with a minimum of ten adjacent 0.2-arcsec pixels at least $1.5\,\sigma$ above the background to provide a source list and then use the APPHOT routine in IRAF to extract 3-arcsec diameter aperture photometry at these positions in each convolved image. These measurements are then aperture corrected assuming a point source, to yield total magnitudes. We report $3\text{-}\sigma$ detection limits in Table 1.

The resolution of the IRAC images is significantly lower than the optical so for source extraction we consider these data separately, although an equivalent procedure is followed. Sources are detected on the 8 μm image with SEXTRACTOR (Bertin & Arnouts 1996) and are required to have a minimum of 4 adjacent 0.9-arcsec pixels at least $2\,\sigma$ above the background. The 8 μm band is chosen so that we can use the IRAC colours to constrain counterparts for otherwise unidentified SMGs ($\S3.2.3$ and Yun et al. 2008). This source list provides positions for the APPHOT routine in IRAF to extract 3.8-arcsec diameter fluxes. We also ensure that all SMGs which are identified in Submillimeter Array (SMA), radio or 24 μm data and have IRAC counterparts in *any* bands are extracted, removing the requirement for an 8 μm detection. The extracted fluxes are corrected for the aperture losses, employing the factors calculated by the SWIRE team (Surace et al. 2007), resulting in total magnitudes, which can be directly compared to our optical catalogue.
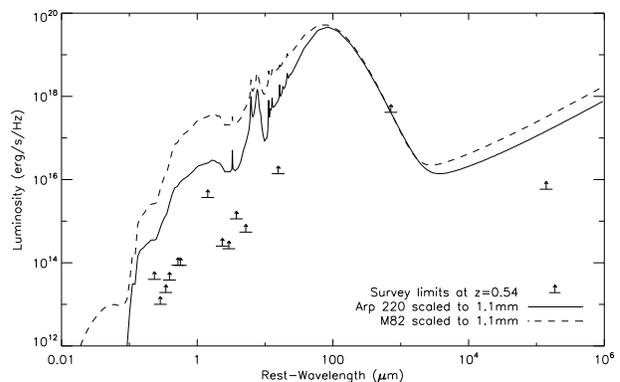

Figure 2. Catalogue detection limits (see Table 1) in each filter for a $z = 0.54$ galaxy overlayed with Arp 220 and M82 SEDs (Silva et al. 1998) scaled to our 3.5σ 1.1 mm catalogue limit. We expect to easily detect counterparts at this redshift suggesting that unidentified SMGs are most likely to be high redshift background galaxies and not cluster members.

3 ANALYSIS AND RESULTS

This study aims to identify 1.1-mm detected ULIRGs in the $z = 0.54$ galaxy cluster MS 0451−03. A priori, based on the space density of ULIRGs at $z \sim 0.5$ (Le Floc'h et al. 2005), and the overdensity of LIRGs in clusters at this redshift (Geach et al. 2006), we expect to find, at most, only a couple of cluster members in our survey. The large background population coupled with this small number of expected members makes this study challenging. Therefore, we focus on techniques to identify sources and confirm cluster membership. Similarly to other SMG studies, a fraction of our sources are unidentified in the radio, mid-IR or optically. However, based on an Arp 220 SED, cluster members which are detectable above our 1.1-mm flux limit are also expected to be brighter than the catalogue limits in all other bands (Fig. 2). Therefore, any unidentified sources are likely to be part of the background population.

Table 2. AzTEC galaxies in the MS 0451−03 field in order of decreasing S/N. Source names correspond to AzTEC positions in the J2000 epoch. SMGs with robust multiwavelength counterparts (§3.2 and Table 3) are shown in bold.

	Source	SNR	Flux (mJy)	Noise (mJy)	Deboosted flux (mJy)
1	**MMJ 045438.96-030739.8[a]**	**6.5**	**8.3**	**1.3**	$6.4^{+1.3}_{-1.4}$
2	**MMJ 045447.55-030018.8[a]**	**5.8**	**6.2**	**1.1**	$4.7^{+1.1}_{-1.1}$
3	**MMJ 045433.57-025204.0[a]**	**5.7**	**7.7**	**1.4**	$5.4^{+1.4}_{-1.5}$
4	**MMJ 045431.56-025957.8[b]**	**5.1**	**5.2**	**1.0**	$3.7^{+1.0}_{-1.1}$
5	**MMJ 045421.55-030109.9**	**5.1**	**5.1**	**1.0**	$3.6^{+1.0}_{-1.2}$
6	**MMJ 045417.49-030306.6**	**4.9**	**5.0**	**1.0**	$3.5^{+1.1}_{-1.2}$
7	**MMJ 045413.35-031204.2[b]**	**4.6**	**6.3**	**1.4**	$3.6^{+1.4}_{-2.0}$
8	**MMJ 045412.72-030043.7**	**4.5**	**4.5**	**1.0**	$2.9^{+1.0}_{-1.3}$
9	**MMJ 045345.31-030552.2**	**4.4**	**4.6**	**1.0**	$2.8^{+1.1}_{-1.4}$
10	**MMJ 045407.14-030033.9**	**4.3**	**4.3**	**1.0**	$2.6^{+1.0}_{-1.4}$
11	MMJ 045358.12-025233.3	4.3	4.3	1.0	$2.6^{+1.0}_{-1.5}$
12	MMJ 045426.76-025806.5	4.2	4.2	1.0	$2.6^{+1.0}_{-1.4}$
13	MMJ 045356.09-025031.4	4.2	5.4	1.3	$2.6^{+1.3}_{-2.2}$
14	MMJ 045424.53-030331.7	4.1	4.2	1.0	$2.4^{+1.0}_{-1.5}$
15	**MMJ 045328.86-030243.3**	**4.1**	**5.0**	**1.2**	$2.5^{+1.2}_{-2.0}$
16	MMJ 045354.64-030004.0	4.0	4.0	1.0	$2.1^{+1.0}_{-1.6}$
17	**MMJ 045431.35-025645.8**	**4.0**	**4.0**	**1.0**	$2.3^{+1.0}_{-1.4}$
18	**MMJ 045411.57-030307.5**	**4.0**	**4.1**	**1.0**	$2.3^{+1.0}_{-1.6}$
19	MMJ 045415.53-025125.0	3.9	4.1	1.0	$2.3^{+1.1}_{-1.6}$
20	MMJ 045345.88-030440.0	3.9	4.0	1.0	$2.2^{+1.0}_{-1.6}$
21	MMJ 045358.49-025601.4	3.9	3.8	1.0	$2.2^{+1.0}_{-1.5}$
22	MMJ 045403.10-025006.8	3.9	4.7	1.2	$2.2^{+1.3}_{-2.0}$
23	MMJ 045357.46-030237.1	3.9	4.0	1.0	$2.1^{+1.0}_{-1.6}$
24	MMJ 045420.10-030658.2	3.8	4.0	1.0	$2.2^{+1.1}_{-1.6}$
25	MMJ 045422.17-030445.8	3.8	3.9	1.0	$2.0^{+1.0}_{-1.7}$
26	**MMJ 045349.69-025807.1**	**3.8**	**3.8**	**1.0**	$2.0^{+1.0}_{-1.6}$
27	**MMJ 045421.17-030740.2**	**3.8**	**3.9**	**1.0**	$1.9^{+1.1}_{-1.7}$
28	MMJ 045345.06-025722.6	3.7	3.7	1.0	$1.9^{+1.0}_{-1.6}$
29	MMJ 045442.54-025455.0	3.7	4.5	1.2	$1.6^{+1.4}_{-1.6}$
30	MMJ 045444.78-030030.9	3.7	3.8	1.0	$1.9^{+1.1}_{-1.6}$
31	MMJ 045411.73-025712.7	3.7	3.6	1.0	$1.8^{+1.0}_{-1.6}$
32	MMJ 045411.17-031019.2	3.6	4.1	1.1	$1.8^{+1.2}_{-1.7}$
33	MMJ 045352.72-030130.9	3.6	3.7	1.0	$2.0^{+1.0}_{-1.6}$
34	MMJ 045454.20-025919.3	3.6	4.6	1.3	$1.5^{+1.5}_{-1.5}$
35	MMJ 045359.27-030327.4	3.5	3.6	1.0	$1.8^{+1.0}_{-1.6}$
36	MMJ 045340.09-030334.2	3.5	3.6	1.0	$1.7^{+1.0}_{-1.6}$

[a] These SMGs were observed with the SMA and detected (§3.2.1).
[b] These SMGs were observed with the SMA but not formally detected (§3.2.1).

3.1 AzTEC catalogue

Millimetre sources are identified as local maxima with S/N ⩾ 3.5 and are selected in the roughly uniform noise ($\sigma \sim 1.1$ mJy, ~ 360-arcmin^2) region of the AzTEC signal-to-noise map (with weights of at least half of the maximum). In Table 2 we present these 36 detections in order of decreasing S/N. Measured source fluxes and their errors are given by the peak pixel value and corresponding noise value respectively; deboosted fluxes are calculated following the method of Perera et al. (2008). We determine the positions of sources on the sub-pixel level by calculating the centroid after weighting pixels close to the brightest pixel according to the square of their fluxes. Fig. 1 shows the Subaru *R*-band image with AzTEC contours of constant S/N and the detected 1.1-mm sources
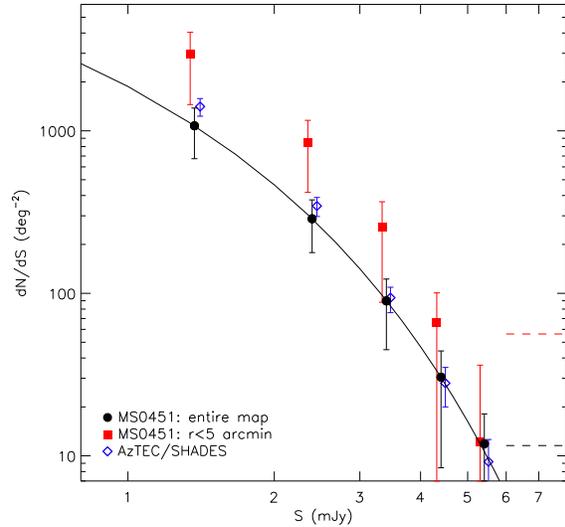

Figure 3. Differential number counts using deboosted fluxes from the AzTEC survey of MS 0451−03 compared to those from the AzTEC/SHADES survey (Austermann et al. 2009b). We see that across the whole area of our survey there is no strong overdensity of 1.1 mm sources in MS 0451−03 compared to the AzTEC/SHADES blank-field survey; hence it is apparent that the majority, but not necessarily the entirety, of the millimetre sources in the cluster field are background galaxies. However, in the central 5 arcmin radius of the map (~ 1.9 Mpc at $z = 0.54$) there appears to be a slight overdensity of sources. This could be due to a combination of the Sunyaev-Zel'dovich effect, gravitational lensing of background sources by MS 0451−03, and potentially a contribution from 1.1 mm cluster members. The solid line is the Schechter function fit to the number counts in the entire AzTEC map, and the dotted lines represent the survey limits - the lower and upper lines represent the whole AzTEC MS 0451−03 field and the central 5 arcmin radius, respectively. For clarity number counts in the central 5 arcmin radius of MS 0451−03 and the AzTEC/SHADES survey are offset slightly in flux.

marked. Based on the analyses of AzTEC data in Scott et al. (2008) and Perera et al. (2008) we expect that 3–4 (8–10%) of the sources in our 3.5σ catalogue are false detections with only ~ 0.5 and 0 amongst those with S/N ⩾ 4.5 and 5 respectively.

To examine whether there is an overdensity of AzTEC galaxies in MS 0451−03 compared to similar field surveys – potentially indicating a significant number of obscured ULIRG cluster members – we calculate the number counts in MS 0451−03 compared to the AzTEC blank-field survey of the SHADES fields (Austermann et al. 2009b). The source number counts and corresponding errors were calculated using the same bootstrap sampling methods as described in Austermann et al. (2009b), employing the AzTEC/SHADES best fit Schechter parameters as a prior. Due to the effects of flux boosting, our catalogue, which is limited at an apparent S/N ratio of 3.5, corresponding to a typical apparent flux of 3.6 mJy, actually contains sources fainter than this limit, allowing us to statistically constrain counts fainter than 3.6 mJy. We also calculate number counts in the central 5 arcmin radius of the AzTEC MS 0451−03 map, by trimming the map to this area and repeating the calculations with the sky model, deboosting, and completeness estimates based on the full maps, since these are not expected to change across the field. The number counts for the whole MS 0451−03 survey area, and the central 5 arcmin (which represents a physical scale of ~ 1.9 Mpc at $z = 0.54$), compared to the AzTEC/SHADES survey are presented in Fig. 3.

Across the whole field MS 0451−03 does not exhibit a source excess at 1.1 mm compared to a blank field. This suggests that, as expected, there is not a dominant population of luminous obscured star-forming galaxies in MS 0451−03. Nevertheless, it is possible that a small number of the sources are still cluster members. Indeed, our number counts analysis (Fig. 3) suggests there may be a small overdensity of sources in the central 5-arcmin radius region of the AzTEC map. Based on integral number counts and their errors at 1.1 mm down to 1 mJy, derived from bootstrap sampling the Posterior Flux Densities of sources (as described in detail in Austermann et al. (2009b)) a tentative overdensity is apparent at the $\sim 1.6\sigma$ level. If real this overdensity could arise from a combination of the Sunyaev-Zel'dovich effect, the gravitational lensing of background sources by the cluster, and potentially 1.1 mm cluster members. To discover whether any of this excess is caused by 1.1-mm bright cluster galaxies we must first accurately locate the counterparts to the 1.1-mm emission.

3.2 Identifying counterparts to AzTEC sources

The large AzTEC beam (18-arcsec FWHM on the JCMT), coupled with the high spatial density of optical sources makes identification difficult unless precise positions are determined for the SMGs. The observed mm/sub-mm emission from SMGs represents rest-frame far-IR emission from dust-reprocessed starlight or AGN activity. Therefore, by exploiting the far-IR–radio correlation (e.g. Condon 1992; Garrett 2002) and the low spatial density of radio sources, it is possible to employ deep ($\sigma \sim 10\,\mu$Jy), high-resolution, interferometric radio observations to determine accurate source positions for $\sim$60–80 per cent of SMGs (e.g. Ivison et al. 2002, 2005, 2007; Chapin et al. 2009). Similarly, 24-μm observations can be used for identification, a method which has proved useful in confirming tentative radio counterparts, or providing positions for a small number of the radio undetected SMGs (e.g. Ivison et al. 2004; Pope et al. 2006; Ivison et al. 2007; Chapin et al. 2009). In addition, mid-IR colours have been used to isolate potential cluster SMGs – although this emission does not track far-IR output and so it is an indirect indicator of the luminous far-IR source (Ashby et al. 2006; Pope et al. 2006; Yun et al. 2008).

An alternative approach is submillimetre interferometry (e.g. Iono et al. 2006; Younger et al. 2007; Cowie et al. 2009), which is preferable to these traditional radio and mid-IR identification methods because it samples the same part of the Spectral Energy Distribution (SED) as our AzTEC imaging. However, sources generally require individual observations due to the small field-of-views of such instruments, commanding prohibitive exposure times to accurately locate all sources in a catalogue.

We employ all three methods in this work, using millimetre interferometry where available, and radio and mid-IR imaging as an alternative. The details of each of these identification methods is discussed in the following sections. In total we identify 18 AzTEC counterparts (50% of the sample; Table 3), of which 14 (39% of the total) also have optical counterparts (Table 4). In Fig. 2 we demonstrate that at $z \sim 0.5$ our multiwavelength observations are deep enough to detect galaxies above our AzTEC flux limit and hence provide counterparts, assuming SEDs typical of Arp 220 or M82. Therefore, our unidentified sample is not expected to contain cluster members. Of the optically-unidentified SMGs, one lies out of the field of the Subaru, CFHT and IRAC observations, two are contaminated by nearby saturated stars and one is fainter than our detection limits at all wavelengths. We discuss the AzTEC galax-

ies and corresponding counterparts on a source by source basis in Appendix A.

3.2.1 SMA detections

The five brightest SMGs presented here were observed at 890 µm with the SMA in October and November 2007. On-source integration times of 5–6 hours were employed, yielding maps with $\sigma_{890\mu\mathrm{m}} \sim 1.6$ mJy. The SMA configuration resulted in a beam of ~ 3 arcsec. These data are discussed in detail in Wardlow et al. (in prep.).

Of the five sources observed with the SMA MMJ 045438.96, MMJ 045447.55 and MMJ 045433.57 were detected with fluxes of 8.4, 5.5 and 8.3 mJy respectively. The remaining two targets, MMJ 045431.56 and MMJ 045413.35, were undetected, but have AzTEC 1.1 mm detections with $\mathrm{SNR} = 5.1$ and 4.6 respectively. Unlike this MS 0451−03 study, previous SMA observations of AzTEC galaxies in the COSMOS field detected all seven targets (Younger et al. 2007). However, the faintest of the COSMOS SMGs has deboosted 1.1 mm flux of 5.2 mJy, compared to 3.7 and 3.6 mJy for MMJ 045431.56 and MMJ 045413.35 respectively. Therefore, based on the deboosted fluxes it is possible that MMJ 045431.56 and MMJ 045413.35 are too faint to be detected in our observations, although there are examples of bright SMGs that are undetected with the SMA (e.g. Matsuda et al. 2007). Alternatively, the lack of SMA counterparts could suggest that either the 890µm to 1.1 mm flux ratios of these sources are lower than expected (i.e. the dust is colder, or they are higher redshift than spectroscopically identified SMGs), that these galaxies exhibit extended far-IR emission on scales $\gg 2$ arcsec ($\gg 16$ kpc at $z = 2$; for example, from a merger-induced starburst), or that the AzTEC beam contains a blend of multiple SMGs. Our radio and SMA observations have similar resolutions, therefore, extended or multiple radio counterparts can indicate the extended or multiple nature of (sub)millimetre emission. Based on the radio emission it is likely that MMJ 045431.56 is composed of multiple (sub)millimetre sources, as discussed in Appendix A. However, MMJ 045413.35 is more likely to be a single resolved (sub)millimetre source, with a lower 890-to-1100 µm ratio than expected. These issues are discussed further in Wardlow et al. (in prep.). We use the positions of the three SMA detected SMGs in the following analysis.

We note that the proposed radio identifications of MMJ 045438.96 and MMJ 045433.57 are coincident with their SMA positions. The other SMA detected galaxy, MMJ 045447.55, lies ~ 9 arcsec from an elliptical galaxy with bright radio and mid-IR emission, which, due to the high fluxes is formally a 'robust' identification, but is unlikely to be the true source of the millimetre emission. MMJ 045431.56 and MMJ 045413.35 which were targeted but not detected with the SMA are identified through radio and mid-IR counterparts respectively.

Table 3. Radio and 24 μm counterparts of AzTEC galaxies in MS 0451−03. All matches within 10-arcsec are listed, those secure identifications at 1.4 GHz or 24 μm with $P \leqslant 0.05$ are shown in bold and tentative associations ($0.05 < P \leqslant 0.10$) are also presented. Images and a discussion of each source are presented in Appendix A.

	Source	1.4GHz position[a] RA (J2000)	Dec	$S_{1.4\mathrm{GHz}}$[b] (μJy)	1.1mm–1.4GHz Separation (arcsec)	$P_{1.4\mathrm{GHz}}$	24μm position[c] RA (J2000)	Dec	$S_{24\mu\mathrm{m}}$[d] (μJy)	1.1mm–24μm Separation (arcsec)	$P_{24\mu\mathrm{m}}$	24μm–1.4GHz[e] Separation (arcsec)
1	**MMJ 045438.96**[f]	**04h54m39s01**	**−03°07′38″5**	**98.0**	**1.51**	**0.003**	**04h54m38s97**	**−03°07′38″0**	**157**	**1.3**	**0.023**	*0.79*
2	**MMJ 045447.55**[g]	**04h54m47s46**	**−03°00′19″2**	**<51**	**-**	**-**	-	-	**<120**	-	-	-
		04h54m48s14	−03°00′14″6	101	9.78	0.032	04h54m48s12	−03°00′14″3	3396	9.56	0.009	*0.46*
3	**MMJ 045433.57**[f]	**04h54m33s55**	**−02°52′04″6**	**93.5**	**0.71**	**0.0008**	**04h54m33s51**	**−02°52′06″8**	**392**	**3.00**	**0.020**	2.28
4	**MMJ 045431.56**[h]	**04h54m31s69**	**−03°00′07″1**	**77.8**	**9.50**	**0.035**	04h54m31s13	−02°59′51″6	485	8.89	0.076	17.62
5	**MMJ 045421.55**	**04h54m21s66**	**−03°01′08″5**	**84.3**	**2.21**	**0.006**	**04h54m21s40**	**−03°01′07″5**	**209**	**3.29**	**0.046**	4.09
6	**MMJ 045417.49**	**04h54m17s27**	**−03°03′03″2**	**189**	**4.74**	**0.010**	04h54m17s24	−03°03′03″7	217	4.76	0.074	*0.58*
7	**MMJ 045413.35**	**04h54m13s36**	**−03°11′58″8**	**78.4**	**5.44**	**0.021**	04fh54m13s38	−03°11′58″9	333	5.31	0.056	*0.29*
8	**MMJ 045412.72**	**04h54m12s79**	**−03°00′43″9**	**58.3**	**1.03**	**0.002**	-	-	**<120**	-	-	-
9	**MMJ 045345.31**	**04h53m45s29**	**−03°05′53″5**	**92.3**	**1.30**	**0.002**	**04h53m45s36**	**−03°05′52″8**	**1393**	**0.86**	**0.0004**	*1.24*
		04h53m45s07	−03°05′56″6	76.9	5.62	0.022						5.71
10	**MMJ 045407.14**	**04h54m07s08**	**−03°00′37″2**	**60.9**	**3.37**	**0.013**	**04h54m07s07**	**−03°00′37″5**	**1120**	**3.76**	**0.007**	*0.39*
12	MMJ 045426.76[i]	04h54m26s86	−02°58′08″0	<51	-	-	-	-	<120	-	-	-
15	**MMJ 045328.86**[j]	-	-	∼51	-	-	**04h53m28s83**	**−03°02′45″9**	**150**	**2.54**	**0.040**	-
17	**MMJ 045431.35**	**04h54m31s71**	**−02°56′45″0**	**89.3**	**5.41**	**0.019**	-	-	<120	-	-	-
18	**MMJ 045411.57**[j]	-	-	∼51	-	-	**04h54m11s66**	**−03°03′08″0**	**185**	**1.55**	**0.016**	-
26	**MMJ 045349.69**	-	-	<51	-	-	**04h53m49s80**	**−02°58′13″9**	**530**	**7.03**	**0.049**	-
27	**MMJ 045421.17**[j]	-	-	∼51	-	-	**04h54m21s14**	**−03°07′46″1**	**464**	**5.92**	**0.045**	-
28	MMJ 045345.06[j]	-	-	∼51	-	-	04h53m45s33	−02°57′18″1	226	6.00	0.095	-
29	MMJ 045442.54[i]	04h54m42s62	−02°54′48″2	<51	-	-	-	-	<120	-	-	-

[a] 1.4 GHz positions have typical uncertainties of ∼ 0.6-arcsec.

[b] 1.4 GHz fluxes have typical errors of 17 μJy.

[c] 24 μm positions have typical uncertainties of ∼ 1.8-arcsec.

[d] 24 μm fluxes have typical errors of 40 μJy.

[e] 24μm–1.4GHz separations consistent with the same counterpart are italicised.

[f] The radio and mid-IR positions agree with the SMA position (§3.2.1)

[g] MMJ 045447.55 is identified from SMA observations (Wardlow et al., 2009b), but a bright elliptical galaxy ∼ 9.6 arcsec from the AzTEC position is also a formal radio and mid-IR identification. We consider the radio and mid-IR galaxy to be a chance association – at $P = 0.05$ we expect 1–2 chance associations in our catalogue.

[h] There is an additonal 176-μJy 24-μm source, with $P = 0.17$, coincident with the radio counterpart of MMJ 045431.56. It is considered related to the AzTEC detection due to the radio identification.

[i] MMJ 045426.76 and MMJ 045442.54 have no radio or mid-IR counterparts but are identified on the basis of their IRAC colours (Yun et al. 2008).

[j] There is a ∼ 3σ radio peak coincident with the 24-μm counterpart.

3.2.2 *Radio and mid-IR identifications*

In this work we use both 1.4-GHz VLA and 24-μm *Spitzer* MIPS observations to locate the AzTEC galaxies in our sample. We identify SMG counterparts independently at radio and mid-IR wavelengths before comparing these for each AzTEC source. In our maps the surface density of radio galaxies is lower than the mid-IR, the positional accuracy is greater (~ 0.6 arcsec compared to ~ 1.8 arcsec), and the link from the radio emission to the far-IR is tighter. Therefore, if the 24 μm and 1.4 GHz identifications disagree we consider the radio position as the more reliable counterpart.

To ensure that no genuine associations are missed we search up to 10 arcsec from each AzTEC position. This corresponds to a $\sim 3\sigma$ search radius for the lowest signal-to-noise ratio (SNR) sources, where σ is the error on AzTEC position, given by $0.6\mathrm{FWHM}(\mathrm{SNR})^{-1}$, and the FWHM is of the instrument beam (Ivison et al. 2007). We reject counterparts with more than 10 per cent probability of being chance associations using the P-statistic of Downes et al. (1986) (see also Pope et al. 2006; Ivison et al. 2007). Counterparts found with $P < 0.05$ are considered robust and those with $0.05 < P < 0.1$ tentative. We present all identifications in Table 3.

3.2.3 *IRAC identifications*

Yun et al. (2008) studied SMGs securely identified with SMA, radio, or 24 μm data and found that they typically have redder IRAC colours than the submillimetre-faint foreground galaxy population. They proposed a selection criteria for SMG counterparts, based on IRAC colours and found that the SMA detected galaxies in their sample, whether radio and mid-IR identified or not, were all recovered by this method. We verify that this selection criteria for our SMA, radio and 24 μm-identified SMG counterparts and use it to search for counterparts to our otherwise unidentified AzTEC sources and identify two further galaxies. Unlike the Yun et al. (2008) SMA-detected SMGs, MMJ 045447.55, our optically, radio and 24μm faint, but SMA-detected SMG, is not detected in any of the IRAC wavebands to the depth of the survey listed in Table 1.

3.3 Redshifts of MS 0451−03 AzTEC galaxies

Our study seeks to identify potential millimetre sources in the cluster population of MS 0451−03. There are spectroscopic observations of 1639 galaxies within our field, but nevertheless none of the AzTEC galaxies have been spectroscopically observed. Therefore, we use photometric methods to separate any potential AzTEC detected cluster members from 'typical' $z \sim 2$ SMGs. We first apply two simple colour tests – the advantage of these is that it is easy to understand the biases in the sample – before applying a more sophisticated photometric redshift analysis. We use the $S_{24\mu\mathrm{m}}/S_{1.1\mathrm{mm}}$ and $S_{1.4\mathrm{GHz}}/S_{1.1\mathrm{mm}}$ flux ratios to estimate the redshifts of identified AzTEC galaxies and then also consider the BzK selection criteria of Daddi et al. (2004) to separate the higher redshift ($z > 1.4$) SMGs from potential cluster members. Finally, we test whether these conclusions are reliable by using the spectroscopic redshifts and multi-wavelength photometry of the SMGs in Borys et al. (2005), and apply these findings to our AzTEC MS 0451−03 sources to obtain photometric redshifts for our galaxies.

3.3.1 *Simple photometric redshift analysis*

In Fig. 4 we plot $S_{24\mu\mathrm{m}}/S_{1.1\mathrm{mm}}$ versus $S_{1.4\mathrm{GHz}}/S_{1.1\mathrm{mm}}$ for AzTEC MS 0451−03 SMGs. For comparison we plot 850 μm sources from Ivison et al. (2007), extrapolated from the observed 850 μm to the equivalent 1.1mm flux assuming a power law spectrum of the form $S_\nu \sim \nu^{3.5}$. As expected both sets of SMGs lie broadly within the same region of colour-colour space, adding confidence to our detections and identifications. The redshift tracks of the local star-forming galaxy Arp 220, and the higher redshift HR10 ($z = 1.44$) (based on the SEDs of Silva et al. (1998)) suggest that the AzTEC galaxies have redshifts of $1 \lesssim z \lesssim 3.5$, in concordance with the SMG population (Chapman et al. 2005). However, potential degeneracy between redshift and dust temperature in the templates makes this method unreliable for identifying cluster galaxies.

We next determine whether any of the SMGs are likely to lie at low redshift and hence potentially be members of MS 0451−03 using the BzK selection of Daddi et al. (2004) to separate $z > 1.4$ galaxies from those at $z < 1$. Of the ~ 70 SMGs with spectroscopic redshifts presented in Chapman et al. (2005) $\sim 80\%$ have $z > 1.4$, suggesting that the BzK selection should enable us to remove the majority of background sources from our sample. Fig. 5 shows the optically identified SMGs in MS 0451−03 which are covered by our B, z and K imaging, in addition to Daddi et al. (2004) selection criteria for high redshift ($z > 1.4$) galaxies; SMGs with $z_{phot} < 1.4$ are highlighted (§3.3.3). It is clear from Fig. 5 that from a BzK selection alone, at least two SMGs are low redshift and therefore potential cluster members; several additional galaxies lie close to the border or have photometric limits which could place them in the low redshift region. Therefore, we next carry out a full photometric redshift analysis of the whole sample using HY-PERZ (Bolzonella et al. 2000) to calculate redshifts for the SMGs

Table 4. Optical and near-IR photometry for the detected SMG counterparts with derived photometric redshifts. Potential cluster members are shown in bold (§3.3.3).

	Source	U	B	V	R	I	z	K	3.6μm	4.5μm	5.8μm	8μm	z_{phot}
1	MMJ 045438.96	> 25.1	25.89±0.04	24.03±0.04	23.29±0.03	22.77±0.03	23.75±1.10	19.88±0.11	20.78±0.05	20.37±0.03	19.92±0.09	20.44±0.07	$3.42^{+0.07}_{-0.05}$
3	MMJ 045433.57	26.92±0.17	25.60±0.04	24.96±0.05	24.02±0.03	23.35±0.04	-	19.27±0.07	20.41±0.03	20.05±0.02	19.72±0.08	20.11±0.05	$2.55^{+0.06}_{-0.09}$
4	MMJ 045431.56	24.04±0.04	24.20±0.02	23.45±0.03	22.71±0.02	21.97±0.03	21.22±0.05	18.32±0.06	20.18±0.03	20.14±0.02	20.15±0.11	20.85±0.10	$0.86^{+0.04}_{-0.03}$
5[a]	**MMJ 045421.55**	**24.92±0.08**	**24.50±0.03**	**23.37±0.03**	**22.31±0.02**	**21.44±0.03**	**21.31±0.09**	**18.81±0.12**	**19.70±0.02**	**19.96±0.02**	**19.43±0.06**	**20.54±0.08**	$\mathbf{0.50^{+0.05}_{-0.10}}$
8	MMJ 045412.72	> 25.1	> 26.6	> 25.8	> 25.1	> 24.2	> 24.2	> 20.1	19.48±0.01	19.03±0.02	18.61±0.03	19.40±0.03	$1.85^{+0.31}_{-0.15}$
10	MMJ 045407.14	22.83±0.03	22.23±0.02	21.69±0.02	21.23±0.02	20.80±0.02	20.64±0.04	19.67±0.08	20.78±0.05	20.37±0.03	19.92±0.09	20.44±0.07	$0.35^{+0.05}_{-0.03}$
12	MMJ 045426.76	> 25.1	27.32±0.11	27.71±0.57	25.53±0.08	23.83±0.05	26.80±4.24	22.39±0.34	21.95±0.13	21.77±0.10	21.37±0.36	21.25±0.15	$0.89^{+0.10}_{-0.10}$
15	MMJ 045328.86	> 25.1	> 26.6	> 25.8	> 25.1	> 24.2	> 24.2	> 20.1	21.08±0.06	20.83±0.04	20.48±0.15	21.48±0.19	$1.87^{+0.62}_{-0.85}$
17	**MMJ 045431.35**	**24.45±0.05**	**24.37±0.03**	**24.23±0.03**	**23.72±0.03**	**23.31±0.04**	**25.94±1.40**	**21.13±0.17**	**22.21±0.17**	**21.97±0.12**	**22.37±1.21**	**22.07±0.33**	$\mathbf{0.60^{+0.11}_{-0.11}}$
18	MMJ 045411.57	24.83±0.05	24.65±0.03	24.23±0.03	23.53±0.03	22.82±0.03	22.68±0.11	22.27±0.37	22.37±0.20	21.78±0.10	21.41±0.37	21.80±0.25	$0.74^{+0.06}_{-0.10}$
26	MMJ 045349.69	26.41±0.14	26.25±0.06	27.72±0.38	26.04±0.10	24.58±0.09	24.35±0.40	> 20.1	-	-	-	-	$1.33^{+0.03}_{-0.10}$
27	MMJ 045421.17	25.42±0.10	25.51±0.04	24.46±0.04	23.56±0.03	23.11±0.04	23.68±0.22	18.82±0.07	20.07±0.02	19.83±0.02	19.15±0.05	20.52±0.08	$1.80^{+0.25}_{-0.26}$
28	MMJ 045354.06	25.61±0.08	25.19±0.03	24.83±0.05	24.68±0.04	24.35±0.07	24.36±0.34	21.63±0.43	-	-	-	-	$1.89^{+0.35}_{-0.84}$
29	MMJ 045442.54	25.00±0.09	26.16±0.05	25.71±0.12	24.61±0.04	23.86±0.05	> 24.2	20.65±0.13	21.59±0.10	21.42±0.07	20.49±0.16	21.31±0.16	$1.09^{+0.15}_{-0.15}$

[a] This is the combined photometry for C1 and C2 as discussed in §3.3.3
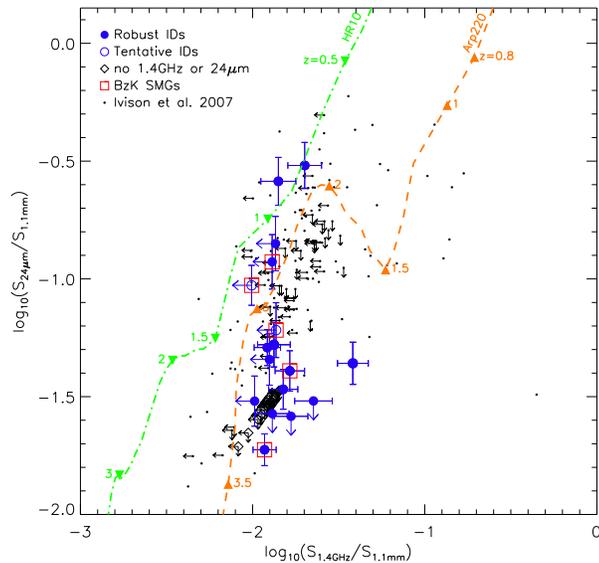
Figure 4. $S_{24\mu m}/S_{1.1mm}$ versus $S_{1.4GHz}/S_{1.1mm}$ for SMGs in the MS 0451−03 field. We differentiate between sources with robust and tentative detections ($0.05 < P \leqslant 0.10$), and highlight SMGs which satisfy the BzK selection criteria of Daddi et al. (2004) (Fig. 5). Sources without both mid-IR and radio detections are plotted at the 3σ detection limit of the respective catalogues (Table 1). For comparison we also plot SHADES identifications (Ivison et al. 2007), converted to expected observed 1.1 mm fluxes as discussed in the text; error bars of this sample are omitted for clarity. Both sets of SMGs lie broadly within the same region of colour-colour space, providing confidence in our identifications. Redshift tracks of the $z = 1.4$ SMG HR 10 and local starburst Arp 220 (based on SEDs from Silva et al. (1998)) suggest that the AzTEC sources generally have $1 \lesssim z \lesssim 3.5$, in concordance with Chapman et al. (2005).

3.3.2 Photometric redshifts of SMGs

Having located the MS 0451−03 SMGs we now need to test whether any are potential cluster members. Photometric redshifts have been calculated for several sets of SMGs using various codes and spectral templates, generally designed for use on 'normal' low redshift galaxies (e.g. Clements et al. 2008). However, SMGs are located at high redshifts and powered by dusty starbursts which can be contaminated by AGN meaning that the stellar templates derived from low redshift galaxies may not be appropriate.

Typically studies of SMGs do not have both spectroscopic and photometric information so testing of photometric redshift results is difficult. Often results from codes such as HYPERZ (Bolzonella et al. 2000) or IMPZ (Babbedge et al. 2004) are compared to those from other, apparently cruder, methods of redshift estimation – such as the radio to far-IR -(sub)-mm spectral indices (e.g. Carilli & Yun 1999; Yun & Carilli 2002; Aretxaga et al. 2003; Clements et al. 2008). There are two main problems with this approach – firstly, the comparison is made with a set of results which themselves are not known to be correct, and secondly, the errors on the comparison redshifts are typically large, such that a general agreement can be confirmed but nothing more. In cases where spectroscopic information has been obtained for a sub-sample of galaxies typically they are small (e.g. Pope et al. 2005).

In this work we expand on previous analyses to examine how well redshifts can be constrained for a spectroscopically confirmed sample of typical SMGs (median $z \sim 2.2$). We employ the sam-
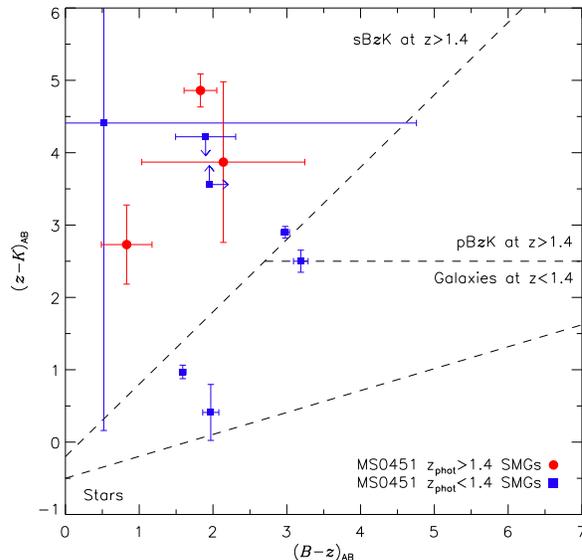
Figure 5. $B - z$ vs. $z - K$ colour-colour plot of the optically identified AzTEC galaxies in MS 0451−03 which lie within the field-of-view of our *B*, *z* and *K* observations. The lines of separation between passive and star-forming $z > 1.4$ BzK galaxies (pBzK and sBzK respectively), $z < 1.4$ galaxies, and stars (Daddi et al. 2004) are shown. Two SMGs occupy the $z < 1.4$ region, suggesting they are potential cluster members. We distinguish between galaxies with $z_{phot} > 1.4$ and $z_{phot} < 1.4$ based on photometric redshifts calculated in §3.3.3. The BzK selection and full photometric analysis broadly agree as to the high and low redshift samples giving more confidence in our ability to isolate millimetre sources in the cluster from the dominant background population. As expected, by this criteria most SMGs are deemed to be actively star-forming.

ple of 12 SMGs from Borys et al. (2005) which have spectroscopic redshifts from Chapman et al. (2003, 2005) and Pope et al. (2008). Photometry in 12 bands from *U* to 8 μm is presented in Borys et al. (2005). We note that SMM J123622.65 has a rest-frame UV/optical spectrum with $z = 2.466$ (Chapman et al. 2005; Swinbank et al. 2004) but mid-IR spectroscopic analysis suggests $z = 1.79 \pm 0.04$ (Pope et al. 2008), therefore, we exclude it from the statistical analyses. We also exclude SMM J123712.05 from the sample as it is undetected at wavelengths shorter than 2 μm and the power-law shape at longer wavelengths means that the redshift cannot be derived.

We use the HYPERZ[2] package (Bolzonella et al. 2000) for our photometric redshift estimates. The program calculates expected magnitudes in the observed filters for given SEDs of a library of model star-formation histories, with different ages, reddening and redshifts; the observed and expected magnitudes are compared in each filter. We use the Bruzual & Charlot (1993) spectral templates provided with the HYPERZ package which represent star-formation histories resulting in SEDs which match local ellipticals (E), Sb, a single burst (Burst) and a constant Star-formation rate (Im). Redshifts between 0 and 7 are considered. SMGs are known to be dusty systems, therefore, we initially allow reddening of $0 \leqslant A_V \leqslant 5$, in steps of 0.2 using the Calzetti et al. (2000) reddening law. Ages of the galaxies are required to be less than the age of the Universe at the appropriate redshift.

In Fig. 6, we compare the spectroscopic with our photomet-

---

[2] We use HYPERZ version 10.0 (http://www.ast.obs-mip.fr/users/roser/hyperz/).
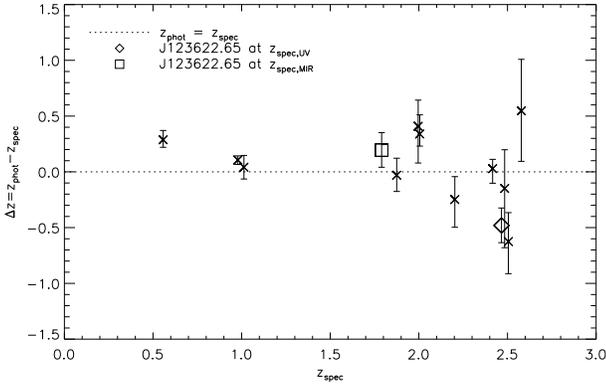
Figure 6. Spectroscopic versus photometric redshifts for the SMGs in Borys et al. (2005). Galaxy SMMJ 123622.65 has rest-frame UV/optical spectra with $z = 2.466$ (Chapman et al. 2005; Swinbank et al. 2004) but mid-IR analysis places it at $z = 1.79 \pm 0.04$ (Pope et al. 2008), therefore, SMMJ 123622.65 is plotted at each redshift. Utilising 12-band photometry results in constraints that are sufficient for separating high-redshift SMGs from those at $z \sim 0.5$.

ric redshifts for the Borys et al. (2005) galaxies; error bars shown are the HYPERZ quoted 99% confidence intervals which represent the 1σ limits more realistically than the HYPERZ quoted 68% intervals for this sample. The average scatter in $\Delta z = z_{\mathrm{phot}} - z_{\mathrm{spec}}$ is 0.27 ± 0.21, although this is smaller for the $z \leqslant 1.5$ SMGs ($\Delta z = 0.15 \pm 0.13$) than for the more distant sample ($\Delta z = 0.32 \pm 0.22$), demonstrating that when testing photometric redshifts of these galaxies it is important to consider a comparison sample with the same redshift distribution as the population under study. Our results are unchanged if we restrict A_V to less than 2.5 although a tighter limit than this does affect the results – increasing Δz.

AGN contamination in the $8\,\mu$m IRAC filter is possible for SMGs (Hainline, L. J. et al. in prep.), therefore we repeat the photometric redshift calculations as above but excluding the $8\,\mu$m data from the analysis. For all the SMGs $\Delta z_{\mathrm{no8\mu m}} \leqslant \Delta z_{\mathrm{allbands}}$ yielding an average scatter $\Delta z = 0.23 \pm 0.22$ for the high redshift ($z > 1.5$) galaxies – consistent with the view that the $8\,\mu$m fluxes are contaminated.

We also find no change if we allow a full range of templates: E, S0, Sa, Sb, Sc, Sd, Burst, and Im spectral types, and minimal change if only we restrict the templates to only Burst and Im models – despite the fact that when the full range of templates is allowed most of the galaxies are best-fit by the burst and elliptical models. We therefore find it unlikely that the addition of any further pure-stellar templates will improve the redshift accuracy.

In this work we are interested in separating low redshift ($z \sim 0.5$; potential cluster member) SMGs from the typical high redshift ($z \sim 2$) population, and it is clear from Fig. 6 that this is possible based on the photometric redshift resolution.

3.3.3 Photometric redshifts of the AzTEC galaxy sample

We use HYPERZ to calculate the redshifts of the SMGs in the field of MS 0451−03 from our optical, near-IR and mid-IR photometry. The Bruzual & Charlot (1993) spectral templates included with HYPERZ are used, and, as discussed in §3.3.2, we consider only the Burst, Elliptical, Sb and constant star-formation rate models, limit reddening to $0 \leqslant A_V \leqslant 5$, and redshifts to $0 \leqslant z \leqslant 7$. Bright, re-

solved galaxies with uncharacteristically high primary photometric redshifts are considered to lie at the calculated secondary solutions.

The redshift estimate of each counterpart is presented in Table 4, and in Fig. 7 we show the SMG photometric redshifts versus AzTEC 1.1-mm fluxes. Although, most of the AzTEC sources are high redshift background galaxies, two – MMJ 045421.55 and MMJ 045431.35 – are possible cluster members, and are discussed further below. We note that as reported by other authors (e.g. Pope et al. 2005) there appears to be a weak trend of redshift with millimetre flux – the brightest millimetre galaxies lie at higher redshifts. Our sample has a median photometric redshift of 1.2 and an interquartile range of $z = 0.7$–1.9 – lower than spectroscopic studies (e.g. Chapman et al. 2005, $\langle z \rangle = 2.2$) but similar to other photometric studies (e.g. $\langle z \rangle = 1.4$; Clements et al. 2008). We note that if we exclude the potential cluster members MMJ 045421.55 and MMJ 045431.35 from this analysis the median redshift of the field SMGs in this study is 1.8 and the interquartile range is $z = 0.9$–1.9.

Although in §3.3.2 we showed that the exclusion of $8\,\mu$m information can sometimes improve the accuracy of photometric redshift estimates of SMGs, the redshifts reported in Table 4 include the $8\,\mu$m photometry. This is because for the galaxies with only IRAC detections the resulting lack of information about the location of the 1.6μm stellar peak means that only weak redshift constraints are possible if we remove the $8\,\mu$m photometry. Critically, the inclusion or exclusion of the $8\,\mu$m information does not affect MMJ 045421.55 and MMJ 045431.35 which still both have photometric redshifts consistent with the cluster.

In Fig. 5 we showed the $B - z$ versus $z - K$ colour-colour plot for AzTEC galaxies in MS 0451−03 and used the BzK selection criteria (Daddi et al. 2004) to separate galaxies above and below $z = 1.4$. We similarly group the SMGs based on the full photometric analysis from HYPERZ and find that both methods broadly agree. In Fig. 7 we show the redshifts and K-band magnitudes of MS 0451−03 SMGs in comparison to the spectroscopic sample of SMGs examined by Smail et al. (2004), and local ULIRGs from Kim et al. (2002) and Stanford et al. (2000). The apparent K-band magnitudes of our AzTEC sample are consistent with their estimated redshifts, when compared with spectroscopic SMG surveys and local ULIRGs, suggesting that our photometric redshifts are reasonable. The general agreement between our photometric redshift analysis, BzK and K-band magnitudes supports the derived redshifts of the AzTEC sources.

The potential cluster members, MMJ 045421.55 and MMJ 045431.35, are discussed in detail here. The other identified SMGs are examined in Appendix A.

MMJ 045421.55 MMJ 045421.55 is identified through radio emission 2.2 arcsec from the AzTEC centroid, which lies between two optical galaxies (2.1 and 1.6 arcsec from the northern (C1) and southern (C2) galaxies respectively). There is also an IRAC source at the location of the radio emission, which appears slightly extended towards C2 (Fig. A1). The three possible explanations for this system are: C1 and C2 are interacting and both millimetre bright; C2 is the millimetre counterpart; or neither C1 nor C2 are responsible for the millimetre emission. Each of these possibilities is discussed below.

Individual photometric analysis of C1 and C2 (excluding the IRAC information) suggests that they are both potential cluster members, and with a separation of 2.6 arcsec - corresponding to ~ 17 kpc at $z = 0.54$ – they could be in the early stages of a merger. Although high-resolution (0.1 arcsec) archival *HST*
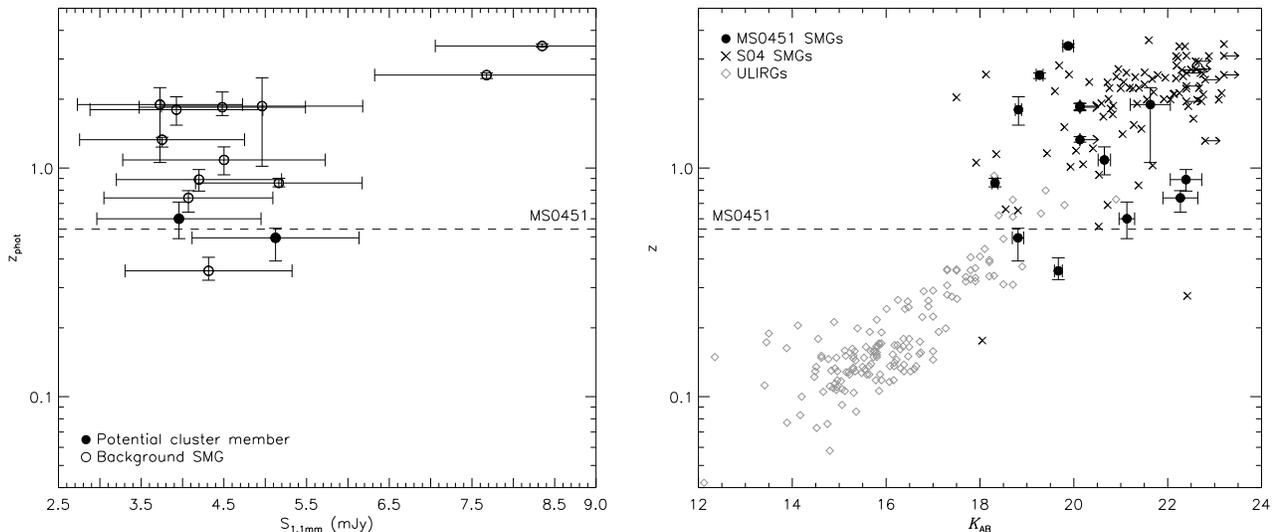
Figure 7. The left-hand panel shows photometric redshifts of SMGs against the 1.1 mm AzTEC fluxes. Two SMGs - MMJ 045421.55 and MMJ 045431.35 - have photometric redshifts consistent with being cluster members and are highlighted; we discuss these two sources in detail in §3.3.3. In the right-hand panel we show redshift versus K-band magnitudes of MS 0451−03 SMGs compared to the spectroscopic sample presented in Smail et al. (2004), and local ULIRGs from Kim et al. (2002) and Stanford et al. (2000). Both datasets occupy the same parameter space suggesting it is unlikely that any of our photometric redshifts are extreme outliers.

F814W imaging shows no evidence of disturbance (Fig. A1), the expected tidal tails can be low surface brightness features, making them difficult to detect. Such interactions are widely known to trigger dusty starbursts in which the radio emission appears to be located between the optical nuclei (e.g. systems similar to VV 114; Frayer et al. 1999; Le Floc'h et al. 2002; Iono et al. 2004).

With the aim of measuring redshifts we targeted C1 and C2 with the ISIS long-slit spectrograph on the WHT during service time in 2009 February. The total integration time was one hour in σ = 1.1-arcsec seeing and standard reduction techniques were employed. A faint continuum was observed (the two targets are blended), but no features suitable for redshift measurement were detectable. A possible faint ($\sim 2\sigma$) emission feature at 7852 Å is visible, which, if real, is most likely to be [OIII] $\lambda5007$ Å at $z = 0.568$ – placing the galaxy in a small group just behind the cluster. However, the feature is tentative and inconclusive.

On the assumption that C1 and C2 lie at the same redshift, and that the millimetre, radio and IRAC fluxes are emitted from a merging system as described above, we combine the optical fluxes from C1 and C2. The optical to near-IR photometric redshift of the whole system is $z = 0.50^{+0.05}_{-0.10}$ which, as shown in Fig. 7, agrees with the z versus K ULIRG trend. Therefore, if C1 and C2 are an interacting system, MMJ 045421.55 a possible cluster member.

The radio counterpart lies only 2.6σ from C2 (compared to 3.5σ from C1), and the IRAC emission of MMJ 045421.55 appears extended towards C2. Therefore, in the situation where C1 and C2 are unassociated we find it most likely that the C2 is the counterpart to the IRAC, radio and millimetre flux. In this case we obtain a photometric redshift of $z = 0.51^{+0.07}_{-0.05}$ – once again placing MMJ 045421.55 in the region of MS 0451−03.

Based on the intrinsic faintness of many SMG counterparts it is feasible that the identified radio and IRAC emission arises from an optically faint background galaxy, unrelated to C1 and C2, and undetectable in our observations. Previous SMG surveys have confused low redshift galaxies with the source of sub-mm emission due

to the lensing of the background source (e.g. Chapman et al. 2002). In these situations it is only possible to distinguish between a lensed background galaxy and a foreground cluster member through the detection of the faint optical counterpart in deeper imaging, or by the detection of CO emission lines.

MMJ 045431.35 The counterpart to MMJ 045431.35 is securely identified 5.4 arcsec from the AzTEC centroid through its radio emission. The source is detected in all our *Spitzer* and ground-based imaging and resolved in the *HST* F814W image into merging galaxies with centroids separated by $\sim$ 1.6 arcsec ($\sim$ 10 kpc at $z = 0.54$) and tidal tails between them (Fig. A1). We suggest that a dusty starburst triggered by the interaction between the two galaxies is causing the millimetre emission from this system. The photometric redshift is calculated as $z = 0.60 \pm 0.11$, making MMJ 045431.35 a possible cluster member.

If MMJ 045421.55 and MMJ 045431.35 are cluster members at $z = 0.54$ SED-fitting suggests they each have $L_{\mathrm{FIR}} \sim 5 \times 10^{11} L_\odot$ and thus SFR$\sim$ 50 M$_\odot$yr^{-1}. We also find that they are colder than typical $z \sim 2$ SMGs, with dust temperatures of $T_d = 15\pm4$ K (for $\beta = 1.5$), or $T_d = 30\pm5$ K (for $\beta = 1.1$), compared to $T_d \sim 40$ K and $\beta = 1.5$ for archetypal SMGs. Such properties are not unprecedented – the spectroscopic survey of SMGs by Chapman et al. (2005) contained examples of sources with equivalent millimetre-to-radio flux ratios at $z \sim 0.5$, suggestive of galaxies containing cold dust. Similarly, in the SCUBA Local Universe Galaxy Survey (SLUGS) Dunne et al. (2000) surveyed local *IRAS*-bright galaxies with SCUBA at 850 µm and utilised the combined *IRAS* and SCUBA photometry for SED fitting. This sample of local galaxies has $T_d = 35.6 \pm 4.9$ K, and $\beta = 1.3 \pm 0.2$. Indeed, cold low-redshift galaxies are easier to detect at 850 µm or 1.1-mm than their hotter counterparts. This is because colder dust produces emission which peaks at longer wavelengths than hot dust. Therefore, we do not find it unreasonable that one or both

of MMJ 045421.55 and MMJ 045431.35 are cluster members at $z = 0.54$ with $T_d \sim 30$ K and $\beta = 1.1$.

If both MMJ 045421.55 and MMJ 045431.35 are members of MS 0451−03, their combined SFR is ~ 100 M$_\odot$yr^{-1} – a significant fraction of the SFR of all the cluster galaxies within 2 Mpc (200 ± 100M$_\odot$yr^{-1}; Geach et al. 2006) MMJ 045431.35 lies ~ 2.6 Mpc from the cluster centre (about half of the turnaround radius), but MMJ 045421.55 is much closer to the centre: ~ 1 Mpc in projection. Notably, both of these systems are most likely mergers. Although not conclusive, if they are both cluster members, this suggests that existing starbursts are not instantaneously suppressed as they are accreted into the cluster environment, and can survive until at least 1 Mpc from the cluster centre. Alternatively the galaxy pairs could have been accreted into the cluster – suggesting that accreted galaxies can retain their gas reserves during infall into clusters (Geach et al. 2009).

3.4 Cluster and field SEDs

We can also investigate obscured star-formation of the general galaxy population in MS 0451−03 below the flux limit of our AzTEC map by stacking fluxes at the positions of known cluster galaxies. Optical galaxies in MS 0451−03 were morphologically classified by Moran et al. (2007b) using the scheme defined by Abraham et al. (1996), which we group into early-types and late-types for this analysis. We also define a mid-IR sample of galaxies which are bright at 24 μm, based on the catalogue of Geach et al. (2006) with $S_{24\mu m} \geqslant 200$ μJy. To reduce contamination we consider only those galaxies with spectroscopic redshifts and to search for environmental dependencies we also examine spectroscopically identified field galaxies. The cluster members are required to have $0.52 < z < 0.56$ and the field population is outside this window. The field samples have median redshifts of 0.58, 0.46, and 0.28 with interquartile ranges of $z = 0.33$–0.82, 0.26–0.62, and 0.20–0.51 for the mid-IR galaxies, late-types and early-types respectively. For each of these six samples we stack the MIPS 24 μm, AzTEC 1.1 mm and VLA 1.4GHz fluxes. We note that the both galaxy samples are optical magnitude limited due to the requirement for a spectroscopic redshift. Therefore, the stacked SEDs may not be representative of the entire population, in particular the most obscured galaxies are likely to fall below the optical magnitude limit. However, we expect such selection effects to equally affect the cluster and field samples allowing us to compare populations between the two density regimes.

Any galaxies within 9 arcsec (the radius of the AzTEC beam) of an AzTEC map pixel with S/N$\geqslant \pm 3.5$ are removed prior to stacking the AzTEC map. The contribution from each AzTEC-faint galaxy is weighted by the inverse of the squared noise at that pixel to calculate the weighted mean 1.1 mm flux of each population. Similarly we calculate the clipped weighted mean radio flux of each sample using our 1.4 GHz VLA map, correcting for bandwidth smearing, and stack 24 μm image in the same way. The stacking parameters are given in Table 5 and the resulting SEDs are presented in Fig. 8.

We fit the mid-IR and late-type galaxies with template SEDs from Dale & Helou (2002) and calculate the corresponding SFRs based on the far-IR luminosity (Kennicutt 1998). Mid-IR cluster galaxies without bright AzTEC counterparts have SFR $= 16.5 \pm 0.6$ M$_\odot$yr^{-1} which is consistent the SFR estimate of 17.0 ± 0.7 M$_\odot$yr^{-1} for the mid-IR field population. In contrast, the late-type galaxies in the field have SFR $= 3.0 \pm 0.3$ M$_\odot$yr^{-1}, compared to SFR $= 2.3 \pm 0.1$ M$_\odot$yr^{-1} in the cluster. Both clus-

ter and field early-type populations are undetected at 1.1 mm and 24 μm and SED fitting to the 24 μm limits suggest, on average, SFR< 0.06 M$_\odot$yr^{-1}.

Since our samples are flux limited, the different redshift distributions will affect the derived SFR. The extent of this effect on our results is tested by calculating an observed SFR for each sample by fitting templates with $S_{24\mu m} = 200$ μJy at the redshift of the galaxies included in the stacks. Due to the generally higher redshift of the field sample, we find that identical mid-IR populations would be observed with SFR 0.74 ± 0.16 times lower in the cluster than the field. In fact the stacked cluster population is observed with SFR 0.97 ± 0.05 times lower than the field population, therefore, to within $\sim 1\sigma$ the mid-IR samples are consistent. However, the equivalent test for late-type galaxies, where the field sample is, on average, lower redshift, suggests that, due to the different luminosity distance, identical populations in our analysis would appear 2.6 times more active in the cluster than in the field. In fact, the cluster late-type galaxies are less active than the field. Therefore, the cluster environment is suppressing star-formation activity in the late-type population.

Geach et al. (2006) estimated the total SFR within 2 Mpc of the core of MS 0451−03 as 200 ± 100 M$_\odot$yr^{-1}, based on converting 24 μm fluxes of colour-selected 24-μm detected galaxies to total IR luminosities with the *average* SED from Dale & Helou (2002). Our analysis presented in this paper includes radio and 1.1 mm data enabling us to better characterise the cluster populations, and by stacking we can probe a fainter population. Within 2 Mpc of cluster core we calculate SFR$> 315 \pm 50$ M$_\odot$yr^{-1} from the spectroscopically confirmed mid-IR and late-type galaxies. To this we can then add 50 M$_\odot$yr^{-1} for MMJ 045421.55, the potential ULIRG within 2 Mpc of the cluster core.

4 CONCLUSIONS

In this study we have investigated the dust-obscured star-forming population of the galaxy cluster MS 0451−03; we utilise 1.1-mm observations to study obscured star-formation in MS 0451−03. We present a $\sigma \sim 1.1$ mJy AzTEC map of the central 0.1 deg^2 of MS 0451−03, within which 36 sources are detected at S/N$\geqslant 3.5$. We use radio, 24 μm, IRAC and SMA observations to precisely locate 18 of these SMGs.

We calculate the reliability of photometric redshifts for SMGs and find that they are able to remove the bulk of background contamination, allowing us to isolate potential cluster members using our optical, near- and mid-IR photometry. Based on these redshifts we find two SMGs which are possible cluster members: MMJ 045421.55 and MMJ 045431.35. These systems are both resolved into close pairs of galaxies by our ground-based and *HST* imaging, suggesting that interactions have triggered their starbursts. If they are cluster members both of these SMGs contain cold dust with $T_d \sim 30$ K, for $\beta = 1.1$ (similar to SLUGS galaxies; Dunne et al. 2000) and have SFRs of ~ 50 M$_\odot$yr^{-1} each.

Geach et al. (2006) compared obscured activity, based on 24μm emission, in MS 0451−03 and Cl 0024+16 at $z = 0.39$, and found that Cl 0024+16 has SFR ~ 5 times that of MS 0451−03 within 2 Mpc of the clusters centres. They show that, taking into account the slightly different redshifts and masses of these two structures, MS 0451−03 is underactive and Cl 0024+16 overactive at 24μm. Therefore, it is likely the other galaxy clusters, including Cl 0024+16, could contain ULIRGs in significantly larger numbers than we find in MS 0451−03.
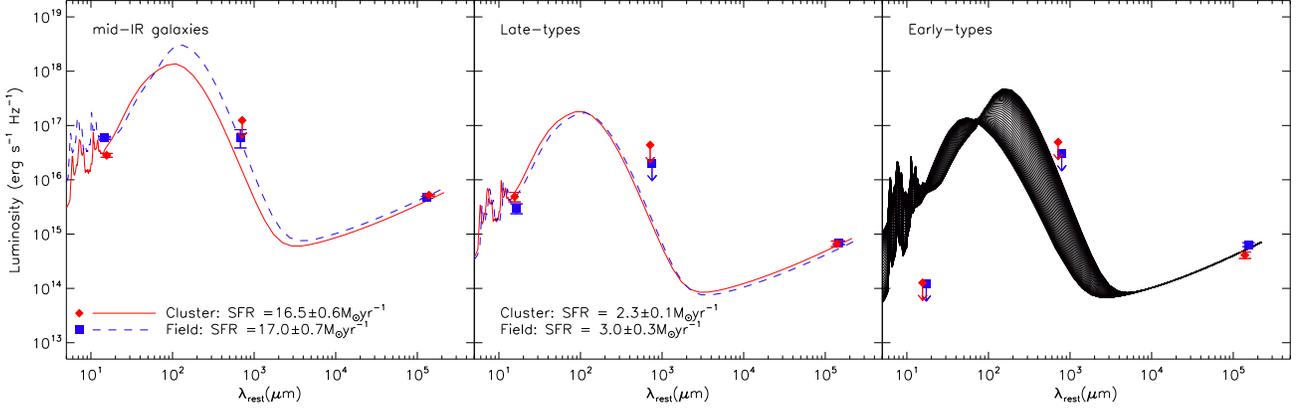
Figure 8. Clipped weighted-average SEDs of the 24μm, late- and early-type populations of MS 0451−03 and the field. In the case of non-detections the 3σ noise limit is marked by arrows. The field populations are calibrated to their mean redshifts of 0.58, 0.46, and 0.39 for the mid-IR galaxies, late- and early-types and respectively. We also show the best-fitting SEDs and corresponding SFRs (Kennicutt 1998) from Dale & Helou (2002) for the mid-IR and late-type galaxies; since the early-type populations are only detected at 1.4 GHz we cannot select one best-fitting SED and instead display all the Dale & Helou (2002) SEDs on this panel. Although the observed populations have similar activity levels, in the late-type galaxies this is due to the flux limits of our observations and the different luminosity distances between the samples. If the cluster and field late-type populations were equivalent, the cluster should have SFR ~ 3 times higher than observed. We deduce that the cluster environment has caused a reduction in the SFR of this population, and that these galaxies are probably in the process of transformation onto the red sequence.

Table 5. Parameters and results of stacking on known cluster and field galaxies in the 24 μm, 1.1 mm and 1.4 GHz images. SFRs are based on SED fits, except for the early-type galaxies, which are based purely on 24 μm detection limits. Non-detections are represented by 3σ limits. Since the samples are flux limited and have various median redshifts we also present the expected observed SFR of the field mid-IR and late-type samples were they to have $z_{median} = 0.54$ (§3.4). Differences between this value and the observed cluster SFR for the late-type galaxies suggests that the cluster late-type population is less active than the field late-type population.

Population	$N_{24\mu m}$[a]	$S_{24\mu m}$[b] (μJy)	$N_{1.1mm}$[a]	$S_{1.1mm}$[b] (μJy)	$N_{1.4GHz}$[a]	$S_{1.4GHz}$[b] (μJy)	z_{median}	SFR ($M_\odot yr^{-1}$)	SFR ($z=0.54$) ($M_\odot yr^{-1}$)
Cluster mid-IR galaxies	14	222 ± 18	14	< 970	15	41.1 ± 1.6	0.54	16.5 ± 0.6	16.5 ± 0.6
Field mid-IR galaxies	84	331 ± 21	94	340 ± 130	89	26.8 ± 1.1	0.58	17.0 ± 0.7	12.6 ± 2.8
Cluster late-type	167	38.4 ± 7.7	131	< 340	162	5.2 ± 0.6	0.54	2.3 ± 0.1	2.3 ± 0.1
Field late-type	315	34.4 ± 7.1	309	< 230	355	8.0 ± 0.6	0.46	3.0 ± 0.3	7.8 ± 1.1
Cluster early-type	148	< 1.0	106	< 390	144	3.2 ± 0.4	0.54	< 0.07	< 0.07
Field early-type	35	< 2.1	32	< 530	40	10.9 ± 0.9	0.28	< 0.03	< 0.19

[a] The number of galaxies used in the stacking – excluding those close to the edge, off-image, or near detected sources

[b] Clipped weighted-average flux

To further investigate the obscured star-forming population which lies below the limit of our AzTEC observations we create composite SEDs of spectroscopically confirmed mid-IR, early- and late-type cluster members and compare them to the corresponding field populations. As expected we find that both early-type populations are undetected at both 24 μm and 1.1 mm and so are unlikely to be actively forming large numbers of stars (< 0.1 $M_\odot yr^{-1}$). The 24 μm galaxies are significantly more active than the morphologically classified late-types with SFRs ~ 15 $M_\odot yr^{-1}$ versus ~ 3 $M_\odot yr^{-1}$ on average. We find that the star-formation activity in the cluster late-type population, compared to a redshift-matched field population is quenched and ~ 3 times lower than expected. Mid-IR galaxies do not show this trend suggesting the more intense activity in these systems is more robust to environmental influences. We find that the total SFR $> 315 \pm 50$ $M_\odot yr^{-1}$ in the central 2 Mpc of MS 0451−03. However, if MMJ 045421.55 is a cluster member it has SFR ~ 50 $M_\odot yr^{-1}$ and lies 1 Mpc from the cluster centre, taking the total SFR within 2 Mpc to $\gtrsim 360$ $M_\odot yr^{-1}$.

REFERENCES

Abraham R. G., van den Bergh S., Glazebrook K., Ellis R. S., Santiago B. X., Surma P., Griffiths R. E., 1996, ApJS, 107, 1

Aretxaga I., Hughes D. H., Chapin E. L., Gaztañaga E., Dunlop J. S., & Ivison R. J., 2003, MNRAS, 342, 759

Ashby M. L. N. et al., 2006, ApJ, 644, 778

Austermann J. E. et al., 2009a, MNRAS, 393, 1573

Austermann J. E. et al., 2009b, preprint (astro-ph/0907.1093)

Babbedge T. S. R. et al., 2004, MNRAS, 353, 654

Bertin E., Arnouts S., 1996, A&AS, 117, 393

Best P. N., 2002, MNRAS, 336, 1293

Biggs A. D., Ivison R. J., 2006, MNRAS, 371, 963

Blain A. W., Barnard V. E., Chapman S. C., 2003, MNRAS, 338, 733

Bolzonella M., Miralles J.-M., Pelló R., 2000, A&A, 363, 476

Borys C., Scott D., Chapman S., Halpern M., Nandra K., Pope A., 2004a, MNRAS, 355, 485

Borys C. et al., 2004b, MNRAS, 352, 759

Borys C., Smail I., Chapman S. C., Blain A. W., Alexander D. M., Ivison R. J., 2005, ApJ, 635, 853

Bower R. G., Lucey J. R., Ellis R. S., 1992, MNRAS, 254, 601

Bruzual A. G., Charlot S., 1993, ApJ, 405, 538

Butcher H., Oemler Jr. A., 1984, ApJ, 285, 426

Calzetti D., Armus L., Bohlin R. C., Kinney A. L., Koornneef J., Storchi-Bergmann T., 2000, ApJ, 533, 682

Carilli C. L., Yun M. S., 1999, ApJ, 513, L13

Chapin E. L. et al., 2009, preprint (astro-ph/0906.4561)

Chapman S. C., Blain A. W., Ivison R. J., Smail I. R., 2003, Nature, 422, 695

Chapman S. C., Blain A. W., Smail I., Ivison R. J., 2005, ApJ, 622, 772

Chapman S. C., Smail I. R., Ivison R. J., Blain A. W., 2002, MNRAS, 335, L17

Clements D. L. et al., 2008, MNRAS, 387, 247

Condon J. J., 1992, ARA&A, 30, 575

Cowie L. L., Barger A. J., Wang W.-H., Williams J. P., 2009, ApJ, 697, L122

Daddi E., Cimatti A., Renzini A., Fontana A., Mignoli M., Pozzetti L., Tozzi P., Zamorani G., 2004, ApJ, 617, 746

Dale D. A., Helou G., 2002, ApJ, 576, 159

De Lucia G. et al., 2007, MNRAS, 374, 809

Donovan D. A. K., 2007, PhD thesis, University of Hawai'i at Manoa

Downes A. J. B., Peacock J. A., Savage A., Carrie D. R., 1986, MNRAS, 218, 31

Dressler A. et al., 1997, ApJ, 490, 577

Dunne L., Eales S., Edmunds M., Ivison R., Alexander P., Clements D. L., 2000, MNRAS

Edge A. C., Ivison R. J., Smail I., Blain A. W., Kneib J.-P., 1999, MNRAS, 306, 599

Frayer D. T., Ivison R. J., Smail I., Yun M. S., Armus L., 1999, AJ, 118, 139

Garrett M. A., 2002, A&A, 384, L19

Geach J. E., Smail I., Best P. N., Kurk J., Casali M., Ivison R. J., Coppin K., 2008, MNRAS, 388, 1473

Geach J. E., Smail I., Moran S. M., Treu T., Ellis R. S., 2009, ApJ, 691, 783

Geach J. E. et al., 2006, ApJ, 649, 661

Gutermuth R. A., Megeath S. T., Myers P. C., Allen L. E., Pipher J. L., Fazio G. G., 2009, ApJS, 184, 18

Holden B. P. et al., 2009, ApJ, 693, 617

Iono D., Ho P. T. P., Yun M. S., Matsushita S., Peck A. B., Sakamoto K., 2004, ApJ, 616, L63

Iono D. et al., 2006, ApJ, 640, L1

Ivison R. J. et al., 2007, MNRAS, 380, 199

Ivison R. J. et al., 2004, ApJS, 154, 124

Ivison R. J. et al., 2002, MNRAS, 337, 1

Ivison R. J. et al., 2005, MNRAS, 364, 1025

Kennicutt Jr. R. C., 1998, ApJ, 498, 541

Kim D.-C., Veilleux S., Sanders D. B., 2002, ApJS, 143, 277

Knudsen K. K., van der Werf P. P., Kneib J.-P., 2008, MNRAS, 384, 1611

Kodama T. et al., 2005, PASJ, 57, 309

Le Floc'h E., Charmandaris V., Laurent O., Mirabel I. F., Gallais P., Sauvage M., Vigroux L., Cesarsky C., 2002, A&A, 391, 417

Le Floc'h E. et al., 2005, ApJ, 632, 169

Matsuda Y., Iono D., Ohta K., Yamada T., Kawabe R., Hayashino T., Peck A. B., Petitpas G. R., 2007, ApJ, 667, 667

Molnar S. M., Hughes J. P., Donahue M., Joy M., 2002, ApJ, 573, L91

Moran S. M., Miller N., Treu T., Ellis R. S., Smith G. P., 2007a, ApJ, 659, 1138

Moran S. M., Ellis R. S., Treu T., Smith G. P., Rich R. M., Smail I., 2007b, ApJ, 671, 1503

Owen F. N., Keel W. C., Ledlow M. J., Morrison G. E., Windhorst R. A., 2005, AJ, 129, 26

Perera T. A. et al., 2008, MNRAS, 391, 1227

Pope A., Borys C., Scott D., Conselice C., Dickinson M., Mobasher B., 2005, MNRAS, 358, 149

Pope A. et al., 2008, ApJ, 675, 1171

Pope A. et al., 2006, MNRAS, 370, 1185

Scott K. S. et al., 2008, MNRAS, 385, 2225

Silva L., Granato G. L., Bressan A., Danese L., 1998, ApJ, 509, 103

Smail I., Chapman S. C., Blain A. W., Ivison R. J., 2004, ApJ, 616, 71

Smail I., Edge A. C., Ellis R. S., Blandford R. D., 1998, MNRAS, 293, 124

Smail I., Ivison R. J., Blain A. W., 1997, ApJ, 490, L5

Stanford S. A., Stern D., van Breugel W., De Breuck C., 2000, ApJS, 131, 185

Surace J. A. et al., 2005, http://swire.ipac.caltech.edu/swire/astronomers/publications.html

Stott J. P., Smail I., Edge A. C., Ebeling H., Smith G. P., Kneib J.-P., Pimbblet K. A., 2007, ApJ, 661, 95

Swinbank A. M., Smail I., Chapman S. C., Blain A. W., Ivison R. J., Keel W. C., 2004, ApJ, 617, 64

Visvanathan N., Sandage A., 1977, ApJ, 216, 214

Wagg J., Owen F., Bertoldi F., Sawitzki M., Carilli C. L., Menten K. M., Voss H., 2009, ApJ, 699, 1843

Webb T. M. A., Yee H. K. C., Ivison R. J., Hoekstra H., Gladders M. D., Barrientos L. F., Hsieh B. C., 2005, ApJ, 631, 187

Wilson G. W. et al., 2008, MNRAS, 386, 807

Wilson J. C. et al., 2003, in Iye M., Moorwood A. F. M., eds, Proc. SPIE. 4841, Instrument Design and Performance for Optical/Infrared Ground-based Telescopes. p. 451

Younger J. D. et al., 2007, ApJ, 671, 1531

Yun M. S., Carilli C. L., 2002, ApJ, 568, 88

Yun M. S. et al., 2008, MNRAS, 389, 333

Zemcov M., Borys C., Halpern M., Mauskopf P., Scott D., 2007, MNRAS, 376, 1073

APPENDIX A: NOTES ON INDIVIDUAL SOURCES

In Fig. A1 we present images centered on each AzTEC source, in order of decreasing S/N. We show Subaru and IRAC colour, and *HST* images, with radio and 24 µm contours. Identified galaxies are labelled and discussed below.

1. MMJ 045438.96: SMA observations of this galaxy confirm the identified radio and mid-IR counterparts. The corresponding red optical and IRAC source at $z_{\rm phot} = 3.42^{+0.07}_{-0.05}$, has a disturbed morphology in the *HST* image.

2. MMJ 045447.55: This galaxy has been located with the SMA but does not have any radio or 24 µm counterparts, or optical or IRAC galaxies at the SMA position. Therefore, MMJ 0455447.57 could be one of a population of very distant SMGs, or be much cooler and more obscured than typical SMGs.

3. MMJ 045433.57: SMA observations confirm the identified radio and mid-IR counterparts, corresponding to an optically faint but near-IR bright galaxy with $z_{\rm phot} = 2.55^{+0.06}_{-0.09}$. The *HST* image shows three components to this galaxy such that a merger is the likely cause of the ULIRG.

4. MMJ 045431.56: We identify a robust extended radio counterpart 9.5 arcsec from the 1.1 mm centroid, which also corresponds to faint mid-IR emission; we consider the corresponding red galaxy at $z_{\rm phot} = 0.86^{+0.04}_{-0.03}$ to be the likely optical counterpart. The *HST* image of the region shows a galaxy with a bright core and a low surface-brightness tail or edge on spiral arm. However, the picture of this SMG is complicated by the presence of a statistically tentative mid-IR counterpart 9.1 arcsec from the 1.1 mm centroid which is unassociated with the aforementioned radio emission. The 24 µm position is coincident with an extended red IRAC galaxy but no optical sources. Further complexity arises from the SMA observation; MMJ 045431.56 was targeted but not formally detected. However, the SMA data does show two potential sources,

close to an extended $\sim 3\sigma$ peak in the radio map, ~ 3.7 arcsec from the AzTEC centroid and unassociated with both the radio and 24 µm counterparts previously discussed. There is also a red IRAC source at this position, and the *HST* image shows two optical galaxies. However, in the IRAC and ground-based optical data the counterpart is blended with a nearby elliptical galaxy.

5. MMJ 045421.55: We find reliable coincident radio and 24 µm counterparts, corresponding to two optical galaxies separated by 2.6 arcsec, which are possible interacting cluster members ($z_{\rm phot} = 0.50^{+0.05}_{-0.10}$). The system is discussed in detail in §3.3.3.

6. MMJ 045417.49: Both mid-IR and strong radio counterparts are detected although the presence of a nearby, bright star prevents multi-wavelength optical and near-IR study. Although the stellar halo is less extended in the *HST* image no counterpart is visible.

7. MMJ 045413.35: The radio and 24 µm identification agrees with a 2–3σ peak in the 890 µm 'dirty' SMA map. Unfortunately this source lies outside of the IRAC and much of the ground-based optical coverage, although a galaxy is detected in the *U*-band and *HST* imaging.

8. MMJ 045412.72: As potentially part of the gravitationally lensed arc from Borys et al. (2004b) this source is discussed fully in Wardlow et al. (2009b). Our optical imaging is too shallow to detect the ERO discussed in Borys et al. (2004b), but radio and extended IRAC emission betrays the likely counterpart.

9. MMJ 045345.31: There are two secure radio and one 24 µm counterparts. One of the radio galaxies corresponds to the 24 µm position. The IRAC source has a red component at the mid-IR/radio position, but it blended with the emission from an optically saturated star making further conclusions difficult. It is unclear whether the 24 µm and radio flux is from the star or a background SMG counterpart which may be the cause of the red component of the IRAC emission.

10. MMJ 045407.14: We find coincident reliable radio and 24 µm counterparts which are located in a red region at the edge of a bright, resolved galaxy which appears disturbed in the *HST* image and has $z_{\rm phot} = 0.35^{+0.05}_{-0.03}$. The morphology of the galaxy suggests that a merger has triggered a dusty starburst region, causing the millimetre emission. The large size and optical brightness support the low redshift of this galaxy, although if the photometric redshift errors are underestimated it could potentially be a cluster member. Similarly, it is also possible that a background galaxy is the source of the millimetre emission. The detection of CO emission lines is required to confirm either scenario.

12. MMJ 045426.76: There are no radio or mid-IR counterparts identified. However, an IRAC galaxy has colours suggestive of SMG emission (Yun et al. 2008), yielding a counterpart with $z_{\rm phot} = 0.89 \pm 0.10$.

15. MMJ 045328.86: A 24 µm counterpart is detected 3.8 arcsec from the AzTEC position, corresponding to an IRAC source, but no detectable optical flux. The IRAC photometry yields $z_{\rm phot} = 1.87^{+0.62}_{-0.85}$. There is coincident faint radio emission ($\sim 3\sigma$) at the position of the 24 µm counterpart, increasing the likelihood that this is the correct identification.

17. MMJ 045431.35: A radio counterpart 4.8 arcsec from the AzTEC position coincides with an pair of merging galaxies which are resolved in the *HST* image and have $z_{\rm phot} = 0.60 \pm 0.11$; this possible cluster ULIRG is discussed further in §3.3.3.

18. MMJ 045411.57: 24-µm emission betrays the source of the millimetre emission as a galaxy with $z_{\rm phot} = 0.74^{+0.06}_{-0.11}$, which is resolved in the *HST* image as an interacting pair, separated by < 1 arcsec. There is faint radio emission ($\sim 3\sigma$) ~ 2.3 arcsec to the northeast of the 24 µm identification, coincident with a red

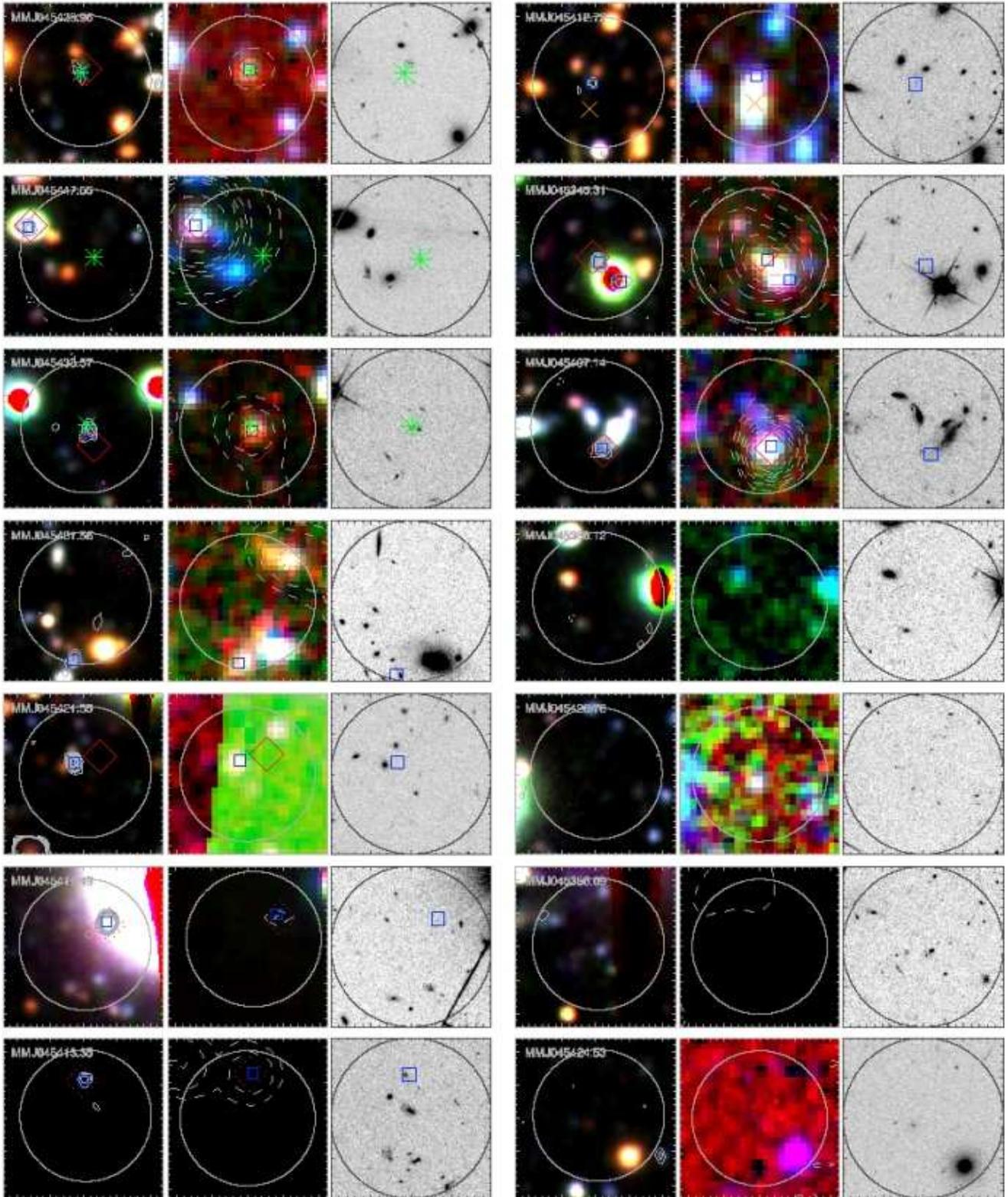**Figure A1.** 25×25 arcsec images centred on each AzTEC galaxy are shown in the left-hand and middle panels; north is up and east is to the left. In the left-hand panel we show Subaru data: *BVR* colour images with solid radio contours at -3 (dotted), 3, 4, 5, 6, 7, 8, 9, $10 \times \sigma$ are overlayed. The middle panel contains true-colour images containing the IRAC $3.6 + 4.5$ (blue), 5.8 (green) and 8.0 μm (red) data; dashed contours present 24 μm flux at 5, 10, 20, 30, 40, 50, 100, 200, ...1000× μJy per pixel and the right-hand panel contains 20×20 arcsec *HST* F814W cutouts centered at the AzTEC position. In all images circles are centred on the AzTEC positions and have 20 arcsec diameter, corresponding to our radio and mid-IR search radius. 24μm and radio counterparts are highlighted with diamonds and squares respectively; dotted symbols represent tentative counterparts (with $0.05 \leqslant P \leqslant 0.10$) and the sizes of the symbols are representative of the typical astrometric errors of these data. We mark the positions of SMA detected sources with stars and X-ray sources (Molnar et al. 2002) with crosses.
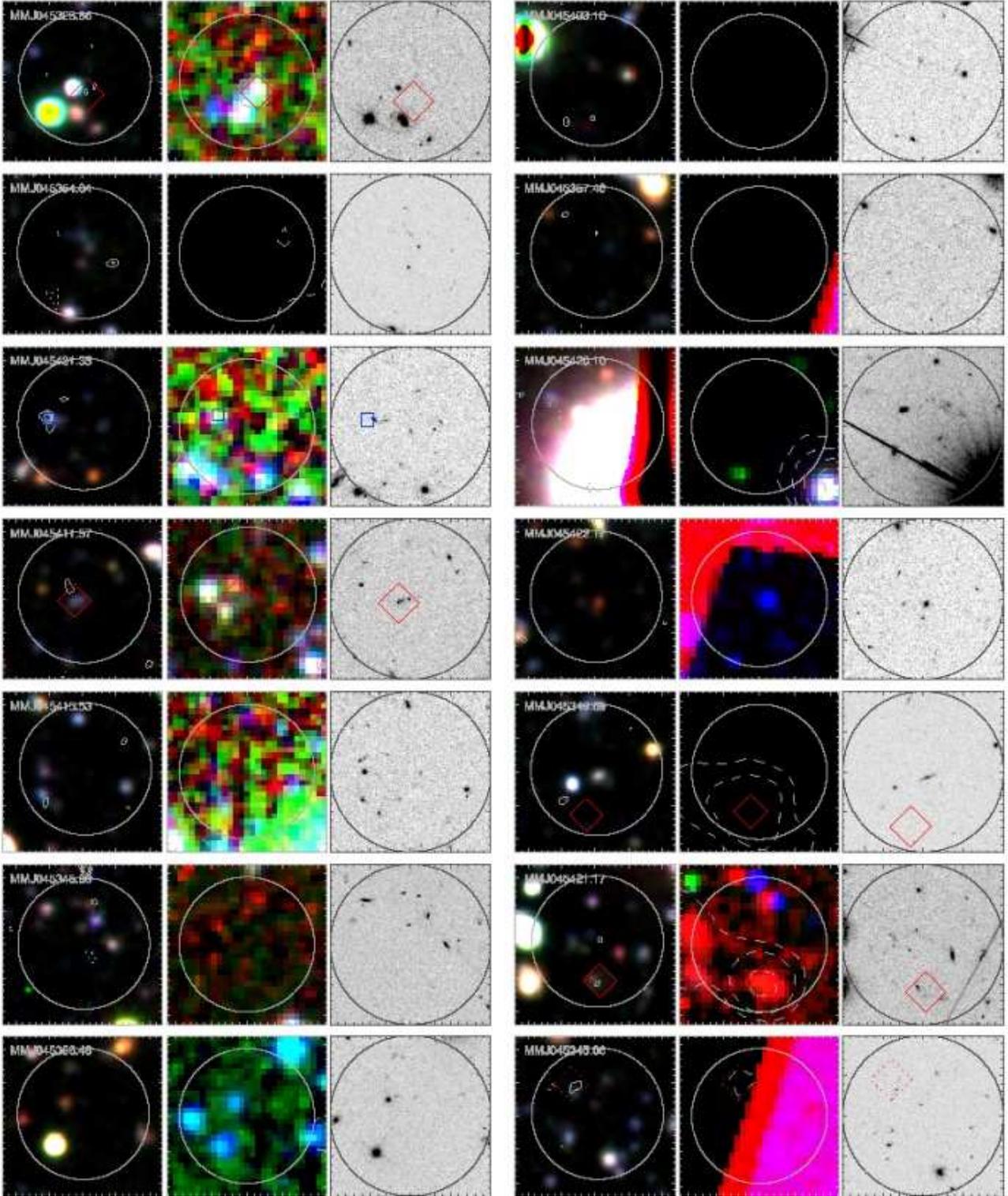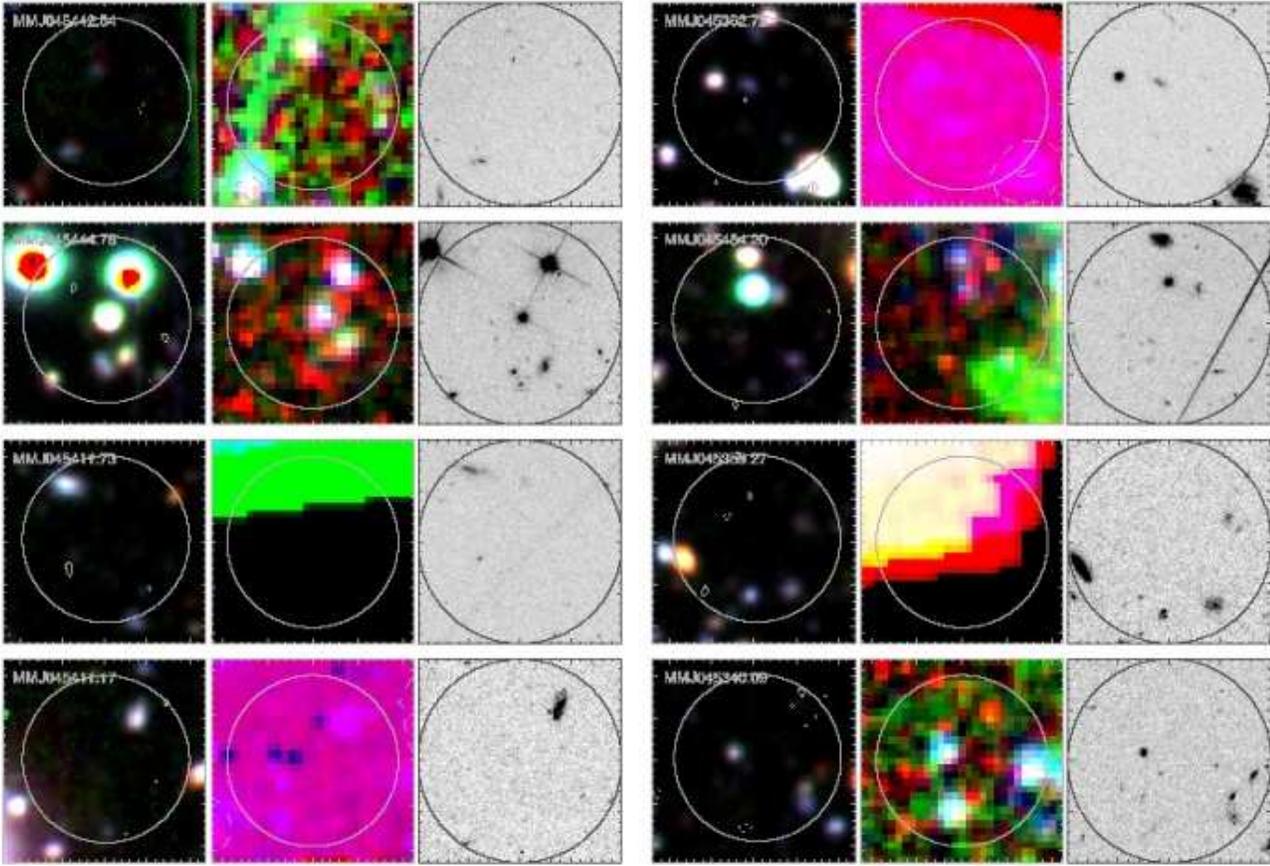
Figure A1 – *continued*

IRAC source. We conclude that the interaction between the optical galaxy pair is producing all of the emission. However, it is possible that the radio and IRAC source is unrelated to the optical emission, in this case we can only constrain the redshift to $z_{\rm phot} > 1.14$.

26. MMJ 045349.69: A faint optical galaxy with $z_{\rm phot} = 1.33^{+0.03}_{-0.10}$ corresponds to the robust mid-IR counterpart. The

galaxy is undetected by *HST* and the region is not covered by our IRAC mosaic.

27. MMJ 045421.17: The mid-IR counterpart is coincident with both faint radio emission and a faint red galaxy at $z_{\rm phot} = 1.80^{+0.25}_{-0.26}$, which the *HST* imaging resolves into a bright nuclear region and some extended emission.

Figure A1 – *continued*

28. MMJ 045345.06: The galaxy is tentatively identified through its mid-IR emission, which is coincident with faint radio flux; our IRAC mosaic does not cover the counterpart, but optical photometry yields $z_{\mathrm{phot}} = 1.89^{+0.35}_{-0.84}$.

29. MMJ 045442.54: Although there are no radio or mid-IR counterparts MMJ 045442.54 is identified from its IRAC colours and the photometry of the corresponding faint galaxy yields $z_{\mathrm{phot}} = 1.09 \pm 0.15$.